Self-formation of concentric zones of telencephalic and ocular tissues and directional retinal ganglion cell axons

Wei Liu [1,2,3]¶, Rupendra Shrestha [1,2,3], Albert Lowe [1,2], Xusheng Zhang [2], Ludovic Spaeth [4]

[1]Department of Ophthalmology and Visual Sciences

[2]Department of Genetics

[3]The Ruth L. and David S. Gottesman Institute for Stem Cell Biology and Regenerative Medicine

[4]Dominick P. Purpura Department of Neuroscience

Albert Einstein College of Medicine, Bronx, NY 10461

¶*Lead Contact.* Email: Wei Liu, wei.liu@einsteinmed.edu

Key words: human pluripotent stem cell, organoid, telencephalon, optic stalk, optic disc, neuroretina, tissue patterning, self-organization, retinal ganglion cell, axon growth and pathfinding, cell surface protein, cell isolation, glaucoma

Summary

The telencephalon and eye in mammals are originated from adjacent fields at the anterior neural plate. Morphogenesis of these fields generates telencephalon, optic-stalk, optic-disc, and neuroretina along an axis. How these telencephalic and ocular tissues are specified coordinately to ensure directional retinal ganglion cell (RGC) axon growth is unclear. Here, we report the self-formation of human telencephalon-eye organoids comprising concentric zones of telencephalic, optic-stalk, optic-disc, and neuroretinal tissues along the center-periphery axis. Initially-differentiated RGCs grew axons towards and then along a path defined by adjacent PAX2+ optic-disc cells. Single-cell RNA sequencing identified expression signatures of two PAX2+ cell populations that mimic optic-disc and optic-stalk, respectively, mechanisms of early RGC differentiation and axon growth, and RGC-specific cell-surface protein CNTN2, leading to one-step purification of electrophysiologically-excitable RGCs. Our findings provide insight into the coordinated specification of early telencephalic and ocular tissues in humans and establish resources for studying RGC-related diseases such as glaucoma.

(150 words)

35 **Introduction**

36 Our understanding of eye and brain development in humans is mostly deduced from animal
37 studies. In mice, fate mapping of the anterior neural plate reveals that the eye field is in rostral
38 regions surrounded anteriorly and laterally by the telencephalic field and caudally and medially
39 by the hypothalamic field, indicating the proximity of their embryonic origins [1]. Subsequent
40 evagination of the eye field generates bilateral optic vesicles and optic stalks; the optic stalks
41 connect the optic vesicles to the forebrain, forming a midline-periphery axis. The optic vesicle
42 then invaginates ventrally, resulting in the formation of double-layered optic cups in which the
43 inner and outer layers develop into the neuroretina and retina pigment epithelium (RPE),
44 respectively. The posterior pole of the optic-cup forms the optic disc (also known as optic nerve
45 head). In the central neuroretina close to the nascent optic disc, retinal ganglion cells (RGCs)
46 start to appear as the optic fissure nearly closes. Early RGC axons find their path toward the
47 optic disc and then enter the optic stalk to reach the brain. Concentrically organized growth-
48 promoting and growth-inhibitory guidance molecules around the optic disc regulate RGC axon
49 growth and pathfinding through multiple mechanisms [2-4]. Coinciding with the optic-cup
50 formation, the surface ectoderm facing the optic vesicle develops into lens. Collectively, the
51 early development of telencephalic and ocular tissues is highly coordinated in mammals.

52 Early telencephalic and eye development is marked and regulated by a group of tissue-specific
53 transcription factors and signal transduction molecules [5]. In mice, Foxg1 is specifically
54 expressed in the presumptive telencephalon and is essential for the development of the cerebral
55 hemispheres [6]. Pax6 is specifically expressed in the eye field and is essential for the
56 development of multiple ocular lineages, such as the neuroretina, lens, and RPE [7-10]. Vsx2 and
57 Mitf are specifically expressed in the neuroretina and RPE, respectively, and are essential for
58 retinal development [11-14]. Pax2 is expressed in the optic stalk, optic vesicles, central neuroretina,
59 and optic disc; Pax2 is essential for optic stalk and nerve development [15-18]. Fgf8 is specifically

60 expressed at the rostral forebrain at early stages, induces Foxg1 expression [19], and regulates
61 telencephalic patterning in a dose-dependent manner [20]. Fgf8 also maintains Pax2 expression
62 in the optic stalk [21], and Fgf8 and Fgf3 coordinate the initiation of retinal differentiation in chicks
63 [22,23]. Despite these findings in vertebrates, it is unclear how telencephalic and ocular tissues are
64 specified in humans.

65 Human organoids are transformative since they enable us to study the mechanisms of cell
66 specification and differentiation directly in humans [24]. Self-organized three-dimensional (3-D)
67 retinal organoids are originally reported by Sasai's group and further improved in follow-up
68 studies [25-33]. We and others have demonstrated that retinal organoids derived from human
69 embryonic stem cells (hESCs) display a stratified structure containing all major types of retinal
70 cells. Although RGCs are differentiated in 3-D retinal organoids, there is no proper RGC axon
71 outgrowth toward the optic disc as seen in vivo since the optic disc-like tissue is missing in
72 retinal organoids. When these organoids are dissociated into single cells or cut into pieces for
73 adherent culture, RGCs generate neurites [34-36]. A variety of brain organoids have been
74 described [37-41]. Although rudimentary ocular tissues are occasionally found in some brain
75 organoids [42], ocular and brain tissues are not patterned along any defined axis. Assembloids, in
76 which retinal, thalamic, and cortical organoids are assembled [32], do not contain any optic disc
77 and stalk tissues. Collectively, RGC axon outgrowth and pathfinding directed by optic disc and
78 stalk tissues in organoids have not been reported. Since RGCs degenerate in glaucoma and
79 cell replacement therapies are actively evaluated, it is imperative to establish models for
80 studying RGC axon growth and pathfinding in humans.

81 Tissue patterning and coordinated specification are fundamental for body plan formation in vivo.
82 Remarkably, concentric zones of trophectoderm, endoderm, mesoderm, and ectoderm [43,44],
83 neural plate and neural plate border [45], and ectodermal cells [46] are self-organized from single

84 pluripotent stem cells, indicating patterning and coordinated specification of these tissues in
85 vitro. Nevertheless, optic disc and stalk tissues are not reported in any of these structures.

86 We hypothesize that coordinated specification from the anterior ectodermal epithelium via
87 morphogen gradients leads to self-organization of telencephalic and ocular tissues, including
88 optic disc- and stalk-like tissues that provide guidance cues for RGC axon growth and
89 pathfinding. In support of this hypothesis, we generated self-formed human telencephalon-eye
90 organoids that comprise concentric zones of anterior ectodermal progenitors (CONCEPT),
91 including tissues mimicking FOXG1+ telencephalon, PAX2+ optic stalk, PAX2+ optic disc,
92 VSX2+ neuroretina, and PAX6+ multi-lineage tissues along the center-periphery axis. We refer
93 these tissues as telencephalon, optic stalk, optic disc, and neuroretina for the sake of gene
94 marker expression, tissue functions, and the ease of description; we do not claim these tissues
95 represent in vivo tissues in all aspects. We call this structure as an organoid since it displays a
96 well-organized structure with cell identities mimicking those tissues in vivo. In CONCEPT
97 organoids, early differentiated RGCs grew their axons toward and then along a path defined by
98 adjacent PAX2+ optic-disc cells. Single-cell RNA sequencing of CONCEPT organoids not only
99 confirmed telencephalic and ocular identities but also discovered expression signatures of cell
100 clusters. We found that PAX2+ optic-disc cells differentially expressed FGF8 and FGF9;
101 inhibition of FGF signaling with an FGFR inhibitor during early RGC differentiation drastically
102 decreased RGCs somas and nearly ablated directional axon growth. Using cell-surface marker
103 CNTN2 identified in our single-cell RNA-sequencing, we developed a one-step method for
104 isolating human electrophysiologically-excitable RGCs under a native condition. Our studies
105 provide deeper insight into the coordinated specification of telencephalic and ocular tissues to
106 ensure guided RGC axon growth in humans and establish resources for studying
107 neurodegenerative diseases such as glaucoma.

108 **Results**

109 **Generation of a telencephalon-eye organoid that is composed of concentric zones of**
110 **anterior ectodermal progenitors (CONCEPT)**

111 The telencephalon and eye in mammals are originated from adjacent fields at the anterior
112 neuroepithelium [1]. Morphogenesis of these embryonic fields leads to the formation of
113 telencephalon, optic stalk, optic disc, and neuroretina along an axis. Early differentiated retinal
114 ganglion cells (RGCs) in the neuroretina grow axons toward the optic disc and then along the
115 optic stalk to reach the brain. How these telencephalic and ocular tissues are specified
116 coordinately to ensure directional RGC axon growth is unclear in humans.

117 Cysts are hollow spheres of an columnar epithelium induced from human pluripotent stem cells
118 through embedding hESC sheets in Matrigel; they are used to generate retinal cells [28,33,47].
119 Nevertheless, developmental potentials of cysts have not been characterized.

120 Using the cysts, here we generate a telencephalon-eye organoid that is composed of concentric
121 zones of anterior ectodermal progenitors (CONCEPT) from cysts (Fig. 1A, B). Cysts were
122 generated as previously described [28,33]. The epithelial structure of cysts was demonstrated by
123 apically localized TJP1::GFP reporter at the lumen (Fig. 1C), consistent with previous findings
124 [28,47]. To assess developmental potentials of cysts, individual cysts were manually picked and
125 then seeded onto the Matrigel-coated surface at low densities (Fig. 1A). After attaching to the
126 culture surface, cysts initially grew as dome-shaped individual colonies. Subsequent culture of
127 the colonies in a KSR medium (see Materials and Methods) led to the self-formation of
128 concentric zones of anterior ectodermal progenitors: an elevated central zone surrounded by
129 multiple zones; this morphology was distinguishable under a steoromicroscope (Fig. 1D) or an
130 inverted microscope. CONCEPT structures were highly reproducible, which is demonstrated by

131 consistent gene expression profiles of multiple CONCEPT organoids in whole culture wells (Fig.
132 S1). If multiple cysts were fused together or cysts for seeding were too big or small, CONCEPT
133 structures were affected or incomplete. CONCEPT structures expressed gene markers for
134 telencephalon and eye in concentric patterns. In mice, Foxg1 is specifically expressed in the
135 E10 telencephalon at high levels; it was also expressed in the optic stalk, invaginating optic cup,
136 and lens at lower levels, with the rostral optic stalk connecting the telencephalic vesicle to the
137 invaginating optic cup (Fig. 1E) [6]; Vsx2 is specifically expressed in the E10.5 neuroretina (Fig.
138 1F); Pax6 is specifically expressed in the E10.5 neuroretina, RPE, lens vesicles, and surface
139 ectoderm (Fig. 1G) [13]. In CONCEPT structures, the expression of FOXG1, VSX2, and PAX6
140 generally exhibited concentric patterns spanning from the center to the periphery (Fig. 1H-O).
141 Similar to FOXG1, telencephalon marker EMX2 [48] was also expressed at the central region (Fig.
142 S1F). PAX6 was expressed in multiple concentric zones at distinct levels, mimicking its
143 expression patterns in multiple ocular tissues in E10.5 mouse eyes (Fig. 1G, J, K, N, O).
144 Therefore, the CONCEPT structure is a telencephalon-eye organoid mimicking telencephalic
145 and ocular tissues in the aspects of cell types and patterning at early stages.

146 Morphogens FGFs and BMPs play crucial roles in patterning the forebrain and eye in vivo. In
147 mice, Fgf8 is specifically expressed at the rostral forebrain at early stages, induces Foxg1
148 expression [19], and regulates telencephalic patterning in a dose-dependent manner [20]. Bmp4 and
149 Bmp7 are expressed in the dorsomedial telencephalon, optic vesicles, and presumptive lens
150 placodes [49-52]. Bmp4 is required for lens induction [50], and Bmp7 is required for proper patterning
151 of the optic fissure [53]. In CONCEPT telencephalon-eye organoids, FGF8, BMP4, and BMP7
152 were expressed in attached cell colonies starting from early stages (Fig. 1P, S, T) and
153 subsequently exhibited circular patterns (Fig. 1R, V, W). At day 10, the expression of BMP4 and
154 BMP7 delineated multiple rings, with a big ring mostly at the center surrounded by numerous
155 small rings (Fig. 1P, S). These observations suggest that the attachment of a single-lumen cyst

156 to the culture surface caused differences in cell behaviors: some cells separated from the
157 original cyst and migrated peripherally; some of the separated cells formed small ring-like
158 structures; the cells that remained at the center formed a big ring-like structure. At day 17,
159 circular patterns of BMP4 and FGF8 emerged (Fig. 1Q, U). At day 25, BMP4, FGF8, and BMP7
160 clearly exhibited circular patterns (Fig. 1R, V, W). Hence, FGFs and BMPs spontaneously form
161 circular gradients, which would dictate coordinated cell specification in CONCEPT
162 telencephalon-eye organoids.

163 **Early differentiated RGCs grow directional long axons toward and then along a path**
164 **defined by PAX2+ cell populations in CONCEPT telencephalon-eye organoids**

165 To assess cell differentiation in CONCEPT telencephalon-eye organoids, we examined marker
166 expression for RGCs, the first type of cells that differentiate in the neuroretina. In mice,
167 transcription factor Pou4f2 is expressed in the early differentiated RGCs and required for the
168 development of a large set of RGCs [54]. Tubb3 is expressed in the somas and axons of
169 differentiating RGCs.

170 In CONCEPT organoids, POU4F2 and TUBB3 were detectable as early as day 17 and
171 increased to higher levels at day 22. RGC somas were marked by POU4F2 and TUBB3 co-
172 expression; RGC axons were marked by TUBB3 expression. Interestingly, RGCs grew
173 directional long axons that followed a circular path (Fig. 2A, B). The circular path of RGC axon
174 outgrowth became more evident in organoids at day 26 (Fig. 2C, D). In mice, the initially
175 differentiated RGCs are adjacent to the optic disc; their axons grow towards the optic disc to exit
176 the eye and then navigate within the optic stalk to reach their targets in the brain; the optic disc
177 and stalk specifically express Pax2 at distinct levels (Fig. 2E-G) [17,55,56]; presumptive optic disc
178 cells expressed VSX2 whereas optic stalk cells do not [13] (Fig. 1F; 2E). In CONCEPT organoids,
179 there were two PAX2+ cell populations that formed two adjacent rings (Fig. 2H-L). POU4F2+

180 RGCs grew TUBB3+ axons toward and then navigated along the adjacent PAX2+ VSX2+ cell
181 population (Fig. 2H-L), mimicking axon growth from the initial RGCs toward the PAX2+ optic
182 disc in vivo. Meanwhile, PAX2+ VSX2- cell population at the inner zone set up an inner
183 boundary of the path for RGC axon growth, mimicking PAX2+ optic stalk that spatially confines
184 RGC axon growth in vivo. Based on these findings, we designate PAX2+ VSX2+ cells and
185 PAX2+ VSX2- cells as the optic disc and optic stalk, respectively. Taken together, our findings
186 demonstrate that RGCs grow directional axons toward and then along a path defined by PAX2+
187 cell populations in CONCEPT telencephalon-eye organoids.

188 **CONCEPT telencephalon-eye organoids contain lens cells that undergo terminal**
189 **differentiation**

190 CONCEPT telencephalon-eye organoids at stages around day 25 contained transparent
191 structures reminiscent of the ocular lens. To determine their cell identity, we performed
192 immunostaining. Starting at day 22, lens markers CRYAA and CRY B were found (Fig. 3A, B)
193 and continuously expressed in the transparent cell structures (Fig. 3C, D). Interestingly, these
194 transparent structures were not stained by DAPI (Fig. 3C-F), indicating denucleation in these
195 lens cells. When CONCEPT organoids were detached using Dispase at around day 28 and
196 continuously grown as suspension cultures, crystal-like clusters with fused transparent spheres
197 were found, and they continuously survived for months (Fig. 3I, J). In mice, terminally-
198 differentiated lens fiber cells are free of organelles and featured by specialized interlocking cell
199 membrane domains shown as ball-and-sockets and protrusions [57]. Using transmission electron
200 microscopy, we found that the crystal-like lens clusters were free of organelles and exhibited
201 ball-and-socket structures (Fig. 3K, L). Taken together, our findings demonstrate that
202 CONCEPT telencephalon-eye organoids contain lens cells that undergo terminal differentiation;
203 FGFs in CONCEPT organoids likely promote terminal lens differentiation as seen in other
204 settings [58].

205 **Single-cell RNA sequencing analysis identifies telencephalic and ocular cell populations**
206 **in CONCEPT telencephalon-eye organoids**

207 To fully characterize cell populations in CONCEPT organoids and the mechanisms underlying
208 RGC axon pathfinding, we performed 10x single-cell RNA sequencing of the organoids at day
209 24, around the stage when RGCs grew long axons toward and along the PAX2+ VSX2+ cell
210 population. Cell Ranger mapping showed that 11158 single cells were sequenced at a depth of
211 27,842 reads and 2,967 genes per cell, and the dataset were then analyzed using Seurat
212 (v3.2.0) [59]. Cell filtration (nFeature_RNA > 200 & nFeature_RNA < 6000 & percent.mt < 20)
213 resulted in 10218 cells with high quality. Cell clustering grouped cells into 14 clusters (Fig. 4A;
214 Tab. 1). In addition, cell cycle scores were plotted using an established method (Fig. 4B) [60].
215 Several cell clusters, *e.g.,* clusters 4, 8, 9, were separated along cell cycle scores (Fig. 4A, B),
216 indicating the differences in cell cycle phases across these cell clusters.

217 We next assessed cell identities using known markers. Mesoderm, endoderm, and neural crest
218 are identified by a group of gene markers [61-64]. In CONCEPT organoids, gene markers for
219 mesoderm (TBXT, GATA2, HAND1), endoderm (GATA1, GATA4, SOX17), and neural crest
220 (SNAI1, SOX10, FOXD3) were not expressed (Fig. S2). In contrast, gene markers for the
221 anterior neuroectoderm were widely expressed. Telencephalic progenitor marker FOXG1 was
222 expressed in clusters 10, 3, 12, 1, 4, 8, 9, 13; retinal progenitor markers PAX6 and VSX2 were
223 expressed in clusters 2, 7, 5, 6, 11 (Fig. 4C-E). Cluster 0 was defined by a group of negative
224 markers (Fig. S3); they expressed both FOXG1+ telencephalic cells and PAX6+ and/or VSX2+
225 retinal cells. In contrast to telencephalon and retinal markers, diencephalon markers (GBX2,
226 WNT3, SOX14) [65,66] and midbrain/hindbrain markers (EN2, PAX7, TFAP2B) [61] were rarely
227 expressed (Fig. S4). Lens markers CRYAA and FOXE3 were expressed in a very small cell
228 population; those denucleated lens cells were not captured in the scRNA-seq since the absence
229 of nucleus prevented active mRNA transcription. Therefore, lens cells did not form a separate

230 cluster probably due to their very low abundance. Taken together, these findings indicate that
231 CONCEPT telencephalon-eye organoids at day 24 are mostly composed of FOXG1+
232 telencephalic cells and PAX6+ and/or VSX2+ retinal cells.

233 We next characterized the FOXG1+ telencephalic cells via assessing differentially expressed
234 genes (DEGs). DEGs in clusters 4, 8, 9, 1 included POU3F3, RGMA, EDNRB, and SOX3,
235 which orthologs in mice are expressed in the pallium. DEGs in clusters 12, 3, 10 included DLX2,
236 RGS16, DLX1, DLL1, DLX6-AS1, NEFL, DCX, and RTN1, which orthologs in mice are
237 expressed in the subpallium (Figs. S5, S6). Therefore, FOXG1+ telencephalic cells in
238 CONCEPT organoids at day 24 comprise cell clusters in both the pallium and subpallium.

239 PAX6+ and/or VSX2+ retinal cells were also grouped into several clusters. VSX2 was
240 expressed in clusters 2, 7, 5, and 0, with cluster 2 at G1 phase, cluster 7 in G1 and S phases,
241 and cluster 5 in S and G2M phases (Fig. 4A, B, E). Cluster 6 did not VSX2 but expressed PAX6
242 and was at the G1 phase, suggesting cells in cluster 6 exited the retinal progenitor cell state and
243 underwent cell differentiation (Fig. 4A, B, D, E). Consistently, cluster 6 differentially expressed
244 RPE markers, e.g., PMEL, HSD17B2, DCT, and MITF (Fig. S7), indicating they were mostly
245 differentiating RPE. Cluster 11 did not express VSX2; instead, it expressed PAX6 and was at
246 the G1 phase (Fig. 4A, B, D, E), suggesting that cells in cluster 11 exited the retinal progenitor
247 cell state and underwent cell differentiation.

248 Taken together, our single-cell RNA sequencing analysis of CONCEPT telencephalon-eye
249 organoids at day 24 confirms their telencephalic and ocular identities, establishing a valuable
250 transcriptomic dataset for mechanistic studies.

251 **Identification of two PAX2+ cell populations that mimic to the optic disc and optic stalk,**
252 **respectively, in the scRNA-seq dataset of CONCEPT telencephalon-eye organoids**

253 To identify PAX2+ cell populations that defined the path for RGC axon outgrowth, we examined
254 PAX2 expression in the dataset. PAX2 was mostly expressed in cluster 2 and subsets of
255 clusters 7, 5, 0, 4, 8, and 9 (Fig. 4A, F). Since clusters 2, 7, 5, and 0 expressed VSX2 (Fig. 4E,
256 F), we deduced that PAX2+ VSX2+ cells in cluster 2 and subsets of clusters 7, 5, and 0
257 corresponded to those PAX2+ VSX2+ cells that defined the path for RGC axon growth (Figs.
258 2H-L). Therefore, these PAX2+ VSX2+ cells in the dataset of single-cell RNA sequencing were
259 assigned as the optic disc (OD) (Fig. 4F). PAX2+ VSX2+ cells also expressed optic disc and
260 optic stalk marker SEMA5A (Fig. 4F, G) [67]. We particularly focused on cluster 2 since PAX2+
261 VSX2+ cells were mostly found in this cluster. Interestingly, COL13A1 was differentially
262 expressed in cluster 2 (Fig. 4H; Fig. S10); in situ hybridization indicates that COL13A1 is
263 specifically expressed in the optic disc of human fetal retinas [68]. These findings firmly support
264 that PAX2+ VSX2+ cells in CONCEPT telencephalon-eye organoids corresponded to optic disc
265 cells in human fetal retinas. Cluster 2 also differentially expressed glaucoma gene CYP1B1,
266 signaling molecules LEFTY2, FGF9, and FGF8 (Fig. 4I-L; Fig. S10). The expression of PAX2,
267 SEMA5A, CYP1B1, LEFTY2, FGF9, and FGF8 in CONCEPT organoids was validated using in
268 situ hybridization (Figs. 1T-V; 5B-E; S10).

269 In contrast, PAX2+ VSX2- cells in subsets of clusters 4, 8, 9 (Fig. 4A, E, F) expressed the optic
270 stalk marker VAX1 (Fig. 4F, M); these cells corresponded to those PAX2+ VSX2- cells that set
271 up the inner boundary of the path for RGC axon growth in CONCEPT organoids (Fig. 2H-L).
272 Therefore, PAX2+ VSX2- cells in subsets of clusters 4, 8, 9 were assigned as the optic stalk
273 (OS) (Fig. 4F). PAX2+ VSX2- optic stalk cells also differentially expressed CNTNAP2, ALDHA3,
274 and LAMP5 (Fig. 4N-P), which orthologs in mice are expressed in the optic stalk/nerve (Fig. S8).
275 Compared to PAX2+ VSX2+ optic disc cells, PAX2+ VSX2- optic stalk cells were closer to
276 telencephalic cells in both the UMAP plot (Fig. 4M-P; Fig. S5A-D) and their positioning in
277 CONCEPT organoids (Fig. 2H-L), mimicking relative positions of telencephalon, optic stalk, and

278 optic disc along the midline-periphery axis in E10.5-E13.5 mouse embryos (Figs. 1E, 2E-G).
279 Consistently, several markers for PAX2+ VSX2- optic stalk cells were also expressed in the
280 telencephalon (Fig. S8). Collectively, we identify two PAX2+ cell populations that mimic the
281 optic disc and optic stalk, respectively, in the scRNA-seq dataset of CONCEPT telencephalon-
282 eye organoids.

283 **Identification of glycosylphosphatidylinositol (GPI)-anchored cell membrane protein**
284 **CNTN2 as a specific marker for developing human RGCs**

285 To identify RGCs in the dataset, we checked the expression of RGC markers. We found that
286 RGC markers ATOH7, POU4F2, SNCG, and CNTN2 were differentially expressed in cluster 11,
287 indicating its RGC identity (Fig. 4A, 4Q-T). CNTN2 caught our attention because it is a GPI-
288 anchored cell membrane protein, which may be used as a native marker for RGC isolation. In
289 literature, Cntn2 is specifically expressed in developing RGCs in mice and chicks [69,70].

290 In CONCEPT at day 25, CNTN2 exhibited an expression pattern very similar to that of TUBB3
291 (Figs. 2, 5). CNTN2 was found in the cell membrane of RGCs that expressed POU4F2 in the
292 cell nucleus (Fig. 5A, D). PAX2+ cells formed inner and outer concentric zones, mimicking the
293 optic stalk and optic disc, respectively. POU4F2+ RGCs formed a dense circular zone adjacent
294 to PAX2+ optic disc cells; POU4F2+ RGCs were sparse in more peripheral areas (Fig. 5B).
295 These findings indicate that early differentiated RGCs were adjacent to PAX2+ optic disc cells.
296 Interestingly, RGCs in the dense POU4F2+ zone grew CNTN2+ axons toward and then along
297 the path defined by adjacent PAX2+ optic disc cells (Fig. 5A-E). In areas where there were a
298 gap in PAX2+ optic disc cells, CNTN2+ axons exited the circular path (diamond arrow in Fig. 5A;
299 a gap between two arrowheads in Fig. 5B, F). In regions where POU4F2+ RGCs were a few
300 hundreds of micrometers away from PAX2+ optic disc cells, RGCs grew axons in centrifugal
301 directions (arrow in Fig. 5C). Very similar findings were found using hiPSCs (Fig. S9), indicating

302 the reproducibility of CONCEPT organoids in multiple cell lines. PAX2+ optic disc cells did not
303 express ALDH1A3; instead, the path for RGC axon growth was bordered by two cell populations
304 that highly expressed ALDH1A3 (Fig. 5G-H). In mice, Aldh1a3 expression was low in
305 differentiating RGCs in the central retina but high in peripheral retinal progenitors and optic stalk
306 (Fig. 5K) [71], consistent with ALDH1A3 expression in CONCEPT organoids (Fig. 5G, H). In mice,
307 Vax1 and Vax2 are expressed in the optic stalk and ventral retina and are jointly required for the
308 optic stalk development [55,72]. In CONCEPT organoids, cells that set up the inner boundary for
309 RGC axon growth also expressed optic stalk marker VAX1/2 (Fig. 5I, J; the antibody recognizes
310 both VAX1 and VAX2). Taken together, our data demonstrate that CNTN2 is a specific cell-
311 surface marker for differentiating human RGCs; RGCs grow axons toward and then along a
312 path that is defined by adjacent PAX2+ VSX2+ ALDH1A3- optic disc cells.

313 **One-step isolation of developing human RGCs via native marker CNTN2**

314 Since cell surface protein CNTN2 was specifically expressed in developing human RGCs, we
315 sought to test whether CNTN2 can be used as a biomarker for isolating human RGCs under a
316 native condition. To that goal, retinal organoids in suspension culture on days 41 - 70 were
317 dissociated using Accutase to generate a single cell suspension, which was then subject to
318 magnetic-activated cell sorting (MACS) with an antibody against CNTN2. From 100 retinal
319 organoids on day 41 to 48, around 385,000 RGCs were isolated. Isolated RGCs were plated
320 onto Matrigel-coated chamber slides for 10-day adherent culture. These cells exhibited neuronal
321 morphology and widely expressed RGC markers TUBB3 and POU4F2 (Fig. 5L). Isolated RGCs
322 tended to form clusters in culture. In contrast to directional axon growth found in CONCEPT
323 organoids, isolated RGCs grew neurites in random directions (Fig. 5L), indicating the
324 differences in axon pathfinding cues between CONCEPT organoids and isolated RGC cultures.
325 RGC neurites were also marked by CNTN2 expression (Fig. 5M). A portion of isolated RGCs
326 expressed POU4F2 but not CNTN2 (Fig. 5M), indicating that CNTN2 was downregulated in

dissociated RGC cultures. Isolated RGCs also expressed RGC markers ISL1, RBPMS, and SNCG (Fig. 5N-P). Collectively, we have developed a one-step method for the isolation of differentiating human RGCs in a native condition.

Isolated RGCs exhibit electrophysiological signature of excitable cells

In order to determine the functional properties of isolated RGCs in culture, we examined their electrophysiological properties using whole-cell patch clamp recordings (Fig. 6, *see Methods*). Using current-clamp configuration, we found that RGCs displayed had a hyperpolarized resting membrane potential (*mean ±SD: -20.1 ±6.4mV*, Fig. 6A). When cells were held at -70 mV by current injection, in most cases (6/9), depolarizing currents steps could trigger an action potential, which were often followed by a depolarization plateau if the current was injected for more than 10ms (Fig. 6B). In voltage clamp recordings we examined the nature of the voltage-gated conductances (*see Methods*). From a holding membrane potential of -80 mV, both inward and outward currents (I_m) were observed in response to depolarizing voltage steps (V_m, Fig. 6C). Outward currents were primarily mediated by voltage-gated potassium channels, as application of 20mM TEA significantly reduced their amplitude (*mean I_K ±SD at 60mV; 964±537 pA in control; 279±201 pA in TEA, U=24.0; p=0.019, two-sided MannWhitneyU test*, Fig. 6D). Conversely, 1μM TTX abolished all inward currents, demonstrating that they were mediated by activation of voltage-gated sodium channels (*mean I_{Na} ±SD at -10mV; -338.2±121 in control; -18.3±13 pA in TTX; U=0.0; p=0.035, two-sided MannWhitneyU test*, Fig. 6E). Taken together, these results indicate that isolated RGCs exhibit functional features traditionally found in excitable cells, such as in neurons.

FGF signaling mediated by FGFRs is required for early RGC differentiation and directional axon growth in humans

350 Directional RGC axon growth toward and then along PAX2+ optic disc cells in CONCEPT
351 organoids could be mediated by signaling molecules secreted from PAX2+ optic disc cells.
352 scRNA-seq analysis identified expression signatures of cluster 2, the major component of
353 PAX2+ optic disc cells (Fig. S10). Interestingly, FGF8 and FGF9 were differentially expressed in
354 cluster 2 (Figs. 4K, 4L; 7A; S10). To assess the roles of FGF8 and FGF9 in CONCEPT
355 organoids, we validated that FGF8 and FGF9 were expressed in PAX2+ optic disc cells of
356 CONCEPT organoids (Fig. 7B-E). TUBB3+ RGC axons grew towards and then along the
357 regions with high-level FGF8 and FGF9 (Fig. 7D, E), suggesting that FGF8 and FGF9 may
358 attract RGC axon growth. FGFR1, FGFR2, FGFR3, MAP2K1, and MAP2K2 were expressed in
359 multiple types of cells in CONCEPT organoids. In RGCs, FGFR1 and MAP2K2 were clearly
360 expressed (Fig. S11), indicating that RGCs expressed the components that transduce FGF
361 signaling. Since FGF8 and FGF9 are probably redundant and it is challenging to inactivate both
362 FGF8 and FGF9 in CONCEPT organoids, we decided to inactivate FGF signaling with
363 FGFR1/2/3 inhibitor PD 161570 during days 17-24, a stage at early RGC differentiation. After
364 the FGFR inhibition, FGF8 expression was grossly unaffected. On the other hand, RGC somas
365 were drastically reduced, and directional axon growth was nearly absent (Fig. 7F-7K). These
366 findings indicate that a) PAX2+ optic disc cells differentially expressed FGF8 and FGF9; b) FGF
367 signaling mediated by FGFRs is required for early RGC differentiation and directional axon
368 growth in humans.

369

370 **Discussion**

371 In this study, we report the self-formation of concentric zones of telencephalic and ocular tissues
372 in CONCEPT telencephalon-eye organoids from human pluripotent stem cells, establishing a
373 model for studying the early development of telencephalic and ocular tissues in humans. RGCs
374 grew axons toward and then along a path defined by PAX2+ cell populations, setting up a
375 model for studying RGC axon pathfinding. We identified expression signatures of cell clusters in
376 CONCEPT organoids using single-cell RNA sequencing and revealed mechanisms of
377 mechanisms of early RGC differentiation and axon growth. Lastly, we established a one-step
378 method for the isolation of human electrophysiologically-excitable RGCs via CNTN2 under a
379 native condition. Our studies not only provide deeper insight into coordinated specification of
380 telencephalic and ocular tissues for directional RGC axon growth in humans, but also generate
381 resources for therapeutic studies of RGC-related diseases such as glaucoma.

382 **The cyst is a radially symmetric epithelium mimicking the anterior ectoderm**

383 Cysts are hollow spheres composed of homogeneous columnar epithelial cells with the apical
384 surface at the lumen. They are induced from pluripotent stem cells via embedding small sheets
385 of hESCs into Matrigel and subsequent growth either in a solid thin film [47] or suspensions [28,33].
386 Cyst growth in suspensions is cost-effective and scalable. The formation of cysts induced by
387 Matrigel mimics the epithelization of the epiblast by the extracellular matrix (ECM) in the
388 blastocyst [73,74].

389 In this study, individual cysts efficiently generate telencephalic and ocular tissues in the absence
390 of any extrinsic factors, indicating their default cell fates of the anterior ectoderm. In literature,
391 anterior neural tissues are generated from re-aggregated single pluripotent stem cells through
392 dual inhibition of Smad signaling [75] or inhibition of Wnt/ß-catenin signaling [27]. Besides that,

393 undirected cultures without extrinsic factors are used for the generation of retinal cultures [29,30,76].
394 In our procedure, we did not add any extrinsic factors; the epithelial structure of cysts and
395 subsequent adherent growth at a low density facilitate neural induction and differentiation. Our
396 findings are consistent with the reports that epiblast cells are epigenetically primed for
397 ectodermal fates [77] and neuroectodermal tissues are the default differentiation from pluripotent
398 stem cells [78,79]. Collectively, cysts mimic the anterior ectoderm in the epithelial structure and cell
399 fates.

400 **Pattern formation and coordinated cell differentiation in CONCEPT telencephalon-eye**
401 **organoids**

402 Tissue patterning is fundamental for the formation of a body plan, which is defined by the
403 anteroposterior, dorsoventral, and left-right axes. Self-formation of CONCEPT telencephalon-
404 eye organoids establishes an efficient way to pattern early telencephalic and ocular tissues
405 along an axis. In CONCEPT organoids on days 22-26, FOXG1+ telencephalon, PAX2+ optic
406 stalk, PAX2+ optic disc, and VSX2+ neuroretinas are positioned along the center-periphery axis,
407 mimicking the relative positions of those tissues in E10.5-13.5 mouse embryos. Our findings
408 indicate that the formation of telencephalic and retinal tissues are highly coordinated, consistent
409 with the prosomere model [80,81]. Collectively, we establish CONCEPT telencephalon-eye
410 organoids for studying the early formation of telencephalic and ocular tissues in humans.

411 The tissue patterning in CONCEPT telencephalon-eye organoids is originated from the
412 attachment of a radially symmetric epithelium to the culture surface for growth as colonies since
413 individual cysts kept in suspensions do not form any apparent tissue patterning. When a floating
414 cyst initially contacted the culture surface, the contact resulted in ECM-cell adhesions. The initial
415 ECM-cell adhesions caused additional ECM-cell contacts in neighboring cells, resulting in the
416 flattening and spreading of a cyst onto the culture surface. Since the cyst is a radially symmetric

417 epithelium, ECM-cell adhesions between the cyst and the culture surface formed sequentially in
418 a concentric manner. Remodeling of cell-cell and ECM-cell adhesions and self-organization
419 underlay the tissue patterning. Molecular events in concentric patterns during the attachment of
420 a cyst onto the culture surface were eventually translated to concentric gradients of morphogens
421 that specify cell fates. The radially symmetric epithelial structure of cysts is important for the
422 formation of a concentric pattern since such pattern would not be generated when amorphous
423 embryoid bodies are attached to the culture surface for growth as colonies. In literature, timed
424 BMP4 treatment is shown to promote neuroretinal differentiation from pluripotent stem cells [82],
425 and FGF8 promotes telencephalic and eye development [5,22]. In our system, BMP4 and FGF8,
426 along with BMP7 and other FGFs, were highly expressed starting at early stages and gradually
427 formed concentric morphogen gradients, which would dictate tissue patterning, resulting in
428 coordinated specification of telencephalic, optic stalk, optic disc, and neuroretinal tissues along
429 the center-periphery axis in CONCEPT telencephalon-eye organoids. Co-culture of these
430 tissues in the concentric zones provides mutual cues for coordinated tissue specification and
431 growth. Nevertheless, anchorage culture of cell colonies prevents three-dimensional
432 morphogenesis as seen in embryos, impeding proper tissue interactions at more advanced
433 stages. When these cell colonies are detached using dispase for suspension culture, retinal
434 progenitor cells self-organize to form protruding, translucent spheres called retinal organoids
435 whereas other types of cells form structures with dark appearance; concentric zones no longer
436 exist [28]. It is conceivable that the simple suspension culture does not have proper physical and
437 chemical supports provided by periocular tissues and other surrounding tissues in vivo and
438 therefore optic stalk cells do not form a tube-like structure. It is a challenge ahead to reconstruct
439 this three-dimensional environment to mimic the morphogenesis in vivo.

440 Concentric patterns of stem cell-derived cultures are also reported in a few other experiments.
441 When dissociated single pluripotent stem cells are grown in micropatterned culture surface at

442 certain cell densities in a medium supplemented with BMP4, concentric zones of progenitors
443 expressing markers for trophectoderm, endoderm, mesoderm, and ectoderm are found [43,44].
444 Cell density and colony geometry dictate cell fate specification from pluripotent stem cells. A
445 concentric gradient of BMP4 activity regulates the patterning [43]. When dissociated single
446 pluripotent stem cells are grown in pre-patterned geometrically confined culture surface in a
447 medium supplemented with dual inhibitors for TGF-β and BMP4, concentric zones of
448 progenitors expressing the markers for neural plate and neural plate border are observed.
449 Morphogenetic cues—cell shape and cytoskeletal contractile force—dictate the patterning of the
450 neural plate and neural plate border via BMP-SMAD signaling [45]. When dissociated single
451 pluripotent stem cells are grown as individual colonies in a medium supplemented with knockout
452 serum replacement, multiple zones of ectodermal cells autonomously form [46]. In all three
453 experiments, dissociated single cells are used to generate cell colonies through either cell re-
454 aggregation or proliferation. In our case, adherent culture of a radially-symmetric epithelium –
455 the cyst – was used to generate CONCEPT organoids. Among the three previous and our
456 experiments, starting cells differ in their developmental potentials, tissue structures, and
457 treatments. Despite the differences, all these organoids comprise concentric zones of distinct
458 cell populations. Formation of CONCEPT telencephalon-eye organoids mimics the coordinated
459 specification of early telencephalic and ocular tissues in humans.

460 **RGC axon pathfinding cues in CONCEPT telencephalon-eye organoids**

461 In the mouse retina, multiple RGC axon guidance cues are concentrically organized around the
462 optic disc, regulating RGC axon growth and exit from the eye through the optic stalk [2]. Early
463 differentiated RGCs are in a short distance from the nascent optic disc, and axons of later
464 differentiated RGCs in more peripheral retinal regions follow the path of the initial axons. It is
465 accepted that the optic-disc regions provide growth-promoting guidance cues whereas
466 peripheral retinal regions provide inhibitory guidance cues [2]. Pax2 is specifically expressed in

467 the ventral optic stalk, optic vesicles, central neuroretina, optic disc, and optic stalk; Pax2 is
468 essential for optic stalk and nerve development in mice [15-17].

469 In CONCEPT telencephalon-eye organoids, coordinated specification of telencephalic and
470 ocular tissues generates PAX2+ optic-disc and optic-stalk cells that define the path for RGC
471 axon growth. To the best of our knowledge, directional RGC axon growth guided by optic-disc
472 and optic-stalk tissues has not been reported.

473 Single-cell RNA sequencing of CONCEPT organoids identified DEGs of PAX2+ optic-disc and
474 optic-stalk cells. Interestingly, FGF8 and FGF9 were differentially expressed in PAX2+ optic-disc
475 cells; inhibition of FGF signaling with an FGFR inhibitor during early RGC differentiation
476 drastically decreased the number of RGC somas and nearly ablated directional axon growth,
477 indicating that early RGC differentiation and directional axon growth require FGFR-mediated
478 FGF signaling in humans. In chicks, Fgf8 and Fgf3 coordinate the initiation of retinal
479 differentiation [22,23]; FGF8 maintains Pax2 expression in optic nerve explants [21]. In mice, FGF8
480 and FGF9 trigger axon outgrowth in motor neuron column explants [83]. Therefore, the roles of
481 FGF signaling in the regulation of early RGC differentiation and directional axon growth in
482 CONCEPT organoids are consistent with literature. Dissecting DEGs of PAX2+ optic-disc cells
483 in CONCEPT telencephalon-eye organoids elucidates the mechanisms of RGC axon growth
484 and pathfinding in humans.

485 RGCs described in this study are still at their early stages in development. One prominent
486 feature of these RGCs are the growth of their axons towards and long the path defined by optic
487 disc cells, which is quite clear in CONCEPT organoids. Optic stalk cells in CONCEPT organoids
488 confine RGC axon growth at inner regions, preventing RGC axons to enter telencephalic areas.
489 We did not observe any clear evidence of synaptic or dendritic connections between RGCs and

490 other cells at tested stages. Engineering assembloids may be needed to establish connections
491 between RGCs and their visual targets.

492 **One-step isolation of developing human RGCs under a native condition**

493 RGCs are degenerated in glaucoma, a major cause of vision impairment in developed countries.
494 Disease modeling and drug discovery to suppress RGC death will have a huge impact on
495 saving vision. The use of human RGC models is critical for therapeutic studies since humans
496 and rodents differ significantly in RGCs. Additionally, cell replacement therapies for glaucoma
497 are extensively evaluated. Therefore, efficient isolation of human RGCs in a native condition will
498 have a substantial impact on therapeutic studies of RGC-related diseases such as glaucoma. In
499 literature, cell surface marker Thy1 is used for the isolation of adult mouse RGCs, but it is
500 unsuccessful in the isolation of RGCs from 3D retinal organoids [84]. A study reports the
501 purification of human RGCs via Thy1 from adherent cultures [85]. Tagging human RGCs with an
502 engineered marker Thy1.2 leads to efficient isolation of human RGCs [84], but may not be
503 unsuitable for clinical uses. Using single-cell RNA sequencing, we identified cell surface protein
504 CNTN2 as a specific marker for developing human RGCs. We isolated human
505 electrophysiologically-excitable RGCs using MACS via CNTN2. Therefore, we establish a one-
506 step method for isolating human RGCs under a native condition, facilitating therapeutic studies
507 for RGC-related retinal diseases such as glaucoma.

508 **Disclosure** – A patent application is pending.

509 **Author Contributions**

510 WL conceived and led the project, performed experiments, analyzed data, drew conclusions,
511 and wrote the paper. RD performed experiments, analyzed data, and edited the paper. AL
512 performed experiments. XZ analyzed the single-cell RNA sequencing dataset. LS designed,

513 performed, and analyzed patch clamp experiments and wrote the section. All authors discussed
514 the results and contributed to the final manuscript.
515
516 **Acknowledgements**
517 We are grateful to Dr. Roy Chuck for support, M.R.G. Stem Cell Institute (supported by
518 NYSTEM C029154) for service, Leslie Cummins and Frank P Macaluso at the Analytical
519 Imaging Facility of AECOM for electron microscopy (supported by P30CA013330), David
520 Reynolds at the Genomics Core of AECOM for the preparation of single-cell libraries, Dr.
521 Kamran Khodakhah for technical support and critical readings, and grants from NEI, NIH
522 (R01EY022645 and R21EY029806 to W.L.). Albert Lowe was supported by training grants
523 T32GM007491 and C30292GG. Ludovic Spaeth was supported by a grant from NIH
524 (5R01NS105470-06 to Dr. Khodakhah).
525

526 **Materials and Methods**

527 **Maintenance of hESCs**

528 ESCRO and IRB committees at AECOM approved the use of hESCs in this project.
529 Undifferentiated H1 hESCs (WiCell WA01) or hiPSCs (Corriell Institute AICS 0023) were grown
530 on Matrigel-coated 6-well plates in mTeSR1 medium and passaged using ReLeSR (STEMCELL
531 technologies) following manufacturer instructions.

532 **Retinal cell differentiation**

533 CONCEPT telencephalon-eye organoids were generated as follows. A humidified incubator at
534 37°C with 5% CO2 was used for cell culture. H1 hESCs or iPSCs that were passaged using
535 ReLeSR two or three days before experiments were detached using Dispase (GIBCO 17105041)
536 and then harvested by centrifugation. After that, the cell pellets were suspended in ice-cold
537 Matrigel. After gelling at 37 °C for 15-20 minutes, the hESC/Matrigel clump was gently
538 dispersed in a N2B27 Medium (DMEM/F12+GlutaMAX (GIBCO):Neurobasal medium (GIBCO)
539 = 1:1, 0.5 x B27 supplement (GIBCO), 0.5 x N2 supplement (GIBCO), 0.1 mM β-
540 mercaptoethanol, and 0.2 mM L-GlutaMax) for floating culture. With the starting day of cell
541 differentiation designated as day 0, cysts with a single lumen formed on day 1. Cysts with a
542 single lumen constituted over 85% of cultures. On day 4 or 5, individual cysts with a diameter at
543 around 150-200 μm were manually picked using a curved Pasteur pipets under an inverted
544 microscope and then seeded onto Matrigel-coated 24-well plates at a density of 2-6 cysts per
545 well. Cysts spontaneously attached to the culture surface and grew. From a time during days
546 13-16, attached cell colonies were grown in a KSR medium (GMEM medium supplemented with
547 10% knockout serum replacement, 1 mM sodium pyruvate, 0.1 mM non-essential amino acids,
548 2 mM l-glutamine, and 55 μM 2-mercaptoethanol; all the culture reagents were from Life

549 Technologies). Culture mediums were changed every two or three days. Overall, the procedure
550 is efficient and robust. Images in the manuscript represent 80-90% of cultures.

551 **Inhibition of FGF signaling in CONCEPT telencephalon-eye organoids with FGFR**
552 **inhibitor PD 161570**

553 To inactivate FGF signaling in CONCEPT organoids, FGFR1/2/3 inhibitor PD 161570 (1 μM;
554 Tocris) was supplemented to the culture medium staring on day 17, with vehicle DMSO as a
555 control. Treated CONCEPT organoids were harvested on day 24 for assays.

556 **Magnetic-activated cell sorting (MACS) of developing human RGCs**

557 Retinal organoids in suspension culture were generated using the established method [28,33]. For
558 each MACS experiment, 84 – 140 retinal organoids at stages of day 41 – 70 were dissociated
559 into single cells using Accutase (GIBCO A1110501). Non-retinal cells were trimmed if there
560 were any. Dissociated single cells were harvested using centrifugation and then incubated for
561 25 minutes at room temperature with MagnaBind goat anti-mouse IgG (ThermoScientific 21354)
562 beads that were previously coupled with a CNTN2 antibody (DSHB 4D7) following manufacturer
563 instructions. Cells bound to the beads were isolated using a magnetic rack and then washed
564 one time with the KSR medium supplemented with antibiotic:Antimycotic (GEMINI 400101)
565 while the tube was still against the magnetic rack. After the wash, the cells were released from
566 the beads via Accutase digestion for 30 minutes and then harvested using centrifugation. The
567 isolated cells were plated onto a chamber slide (ibidi 80826, ibidiTreat μ-Slide 8 Well, coated
568 with poly-ornithine and Matrigel, 30,000-50,000 cells/200 μl/well) in BrainPhys neuronal medium
569 (Stem Cell Technology 05790) supplemented with N2 and B27 (GIBCO 17502001, A3582801).
570 From 100 retinal organoids on day 41 to 48, around 385,000 RGCs were isolated. After 10 days

571 of culture in chamber slides, RGCs were fixed in 4% paraformaldehyde (PFA) for 10 minutes
572 and then processed for immunostaining.

573 **Immunostaining, antibodies, and light microscopy**

574 CONCEPT telencephalon-eye organoids were fixed in 4% PFA for 15-30 minutes at room
575 temperature and processed for immunostaining. See Supplemental Information for details.

576 **In situ hybridization**

577 DIG-labeled anti-sense RNA probes for in situ hybridization were generated via in vitro
578 transcription using a DIG RNA labeling kit (Millipore Sigma-Aldrich 11175025910). See
579 Supplemental Information for details. To assess the in vivo expression of DEGs identified by
580 single-cell RNA sequencing, in situ hybridization images of their mouse orthologs in E14.5
581 mouse brains were downloaded from a public database [86] (https://gp3.mpg.de/) with permission
582 and then assembled in supplemental Figs.

583 **Electron microscopy (EM)**

584 EM was performed by Analytical Imaging Facility in Albert Einstein College of Medicine with a
585 standard method. Lens cell clusters were fixed in 0.1M Cacodylate buffer containing 2%
586 paraformaldehyde and 2.5% glutaraldehyde for 60 minutes at room temperature and then
587 processed for EM.

588 **Single-cell RNA sequencing**

589 CONCEPT telencephalon-eye organoids at day 24 from one culture well were dissociated into
590 single cells using activated Papain (Worthington Biochemical Corporation LS003126) following
591 manufacturer's instructions. Then, 10,000 dissociated cells were captured using Chromium

Controller (10x Genomics), followed by library preparation using Single Cell 3' version 3.1 kit (10x Genomics) following manufacturer's instructions. The library was sequenced in one lane of Illumina HiSeq (2x150 bp) in GeneWIZ company.

Fastq sequences were mapped to the human genome (GRCh38-3.0.0) using CellRanger (3.1.0) to generate a count matrix, which was then analyzed using the Seurat Package (v3.2.0) [59]. Sequenced cells were filtered (nFeature_RNA > 200 & nFeature_RNA < 6000 & percent.mt < 20), resulting in 10218 cells with high quality. Dimension reduction and clustering were performed using the following functions: *NormalizeData, FindVariableFeatures, ScaleData, RunPCA, ElbowPlot, FindNeighbors (dims = 1:17),* and *FindClusters (resolution = 0.5).* Differentially expressed genes were identified using the function *FindAllMarkers (only.pos = FALSE, min.pct = 0.25, logfc.threshold = 0.25)*.

Whole-cell patch clamp recordings of isolated RGCs in culture.

Standdard methods were used. See Supplemental Information for details.

Statistical analysis

Statistical analysis in DEG identification was performed using the Seurat Package (v3.2.0) [59]. Adjusted p-values were shown.

Data availability

Single-cell RNA sequencing data of CONCEPT telencephalon-eye organoids at day 24 is available in Gene Expression Omnibus (http://www.ncbi.nlm.nih.gov/geo) using the accession number GSExxx.

614 **Reference:**

615 1. Inoue, T., Nakamura, S., and Osumi, N. (2000). Fate mapping of the mouse
616 prosencephalic neural plate. Dev Biol *219*, 373-383. 10.1006/dbio.2000.9616.
617 2. Oster, S.F., Deiner, M., Birgbauer, E., and Sretavan, D.W. (2004). Ganglion cell axon
618 pathfinding in the retina and optic nerve. Semin Cell Dev Biol *15*, 125-136.
619 10.1016/j.semcdb.2003.09.006.
620 3. Erskine, L., and Herrera, E. (2007). The retinal ganglion cell axon's journey: insights into
621 molecular mechanisms of axon guidance. Dev Biol *308*, 1-14.
622 10.1016/j.ydbio.2007.05.013.
623 4. Erskine, L., and Herrera, E. (2014). Connecting the retina to the brain. ASN Neuro *6*.
624 10.1177/1759091414562107.
625 5. Wilson, S.W., and Rubenstein, J.L. (2000). Induction and dorsoventral patterning of the
626 telencephalon. Neuron *28*, 641-651. S0896-6273(00)00171-9 [pii].
627 6. Xuan, S., Baptista, C.A., Balas, G., Tao, W., Soares, V.C., and Lai, E. (1995). Winged
628 helix transcription factor BF-1 is essential for the development of the cerebral
629 hemispheres. Neuron *14*, 1141-1152. 10.1016/0896-6273(95)90262-7.
630 7. Zuber, M.E., Gestri, G., Viczian, A.S., Barsacchi, G., and Harris, W.A. (2003).
631 Specification of the vertebrate eye by a network of eye field transcription factors.
632 Development *130*, 5155-5167. 10.1242/dev.00723.
633 8. Marquardt, T., Ashery-Padan, R., Andrejewski, N., Scardigli, R., Guillemot, F., and
634 Gruss, P. (2001). Pax6 is required for the multipotent state of retinal progenitor cells. Cell
635 *105*, 43-55.
636 9. Ashery-Padan, R., Marquardt, T., Zhou, X., and Gruss, P. (2000). Pax6 activity in the
637 lens primordium is required for lens formation and for correct placement of a single
638 retina in the eye. Genes Dev *14*, 2701-2711. 10.1101/gad.184000.
639 10. Baumer, N., Marquardt, T., Stoykova, A., Spieler, D., Treichel, D., Ashery-Padan, R.,
640 and Gruss, P. (2003). Retinal pigmented epithelium determination requires the redundant
641 activities of Pax2 and Pax6. Development *130*, 2903-2915.
642 11. Horsford, D.J., Nguyen, M.T., Sellar, G.C., Kothary, R., Arnheiter, H., and McInnes, R.R.
643 (2005). Chx10 repression of Mitf is required for the maintenance of mammalian
644 neuroretinal identity. Development *132*, 177-187. dev.01571 [pii]
645 10.1242/dev.01571.
646 12. Rowan, S., Chen, C.M., Young, T.L., Fisher, D.E., and Cepko, C.L. (2004).
647 Transdifferentiation of the retina into pigmented cells in ocular retardation mice defines a
648 new function of the homeodomain gene Chx10. Development *131*, 5139-5152.
649 10.1242/dev.01300
650 131/20/5139 [pii].
651 13. Liu, W., Lagutin, O., Swindell, E., Jamrich, M., and Oliver, G. (2010). Neuroretina
652 specification in mouse embryos requires Six3-mediated suppression of Wnt8b in the
653 anterior neural plate. J Clin Invest *120*, 3568-3577. 10.1172/JCI43219.
654 14. Bharti, K., Gasper, M., Ou, J., Brucato, M., Clore-Gronenborn, K., Pickel, J., and
655 Arnheiter, H. (2012). A regulatory loop involving PAX6, MITF, and WNT signaling
656 controls retinal pigment epithelium development. PLoS Genet *8*, e1002757.
657 10.1371/journal.pgen.1002757.

15. Torres, M., Gomez-Pardo, E., and Gruss, P. (1996). Pax2 contributes to inner ear patterning and optic nerve trajectory. Development *122*, 3381-3391.
16. Macdonald, R., Scholes, J., Strahle, U., Brennan, C., Holder, N., Brand, M., and Wilson, S.W. (1997). The Pax protein Noi is required for commissural axon pathway formation in the rostral forebrain. Development *124*, 2397-2408.
17. Martinez-Morales, J.R., Signore, M., Acampora, D., Simeone, A., and Bovolenta, P. (2001). Otx genes are required for tissue specification in the developing eye. Development *128*, 2019-2030.
18. Schwarz, M., Cecconi, F., Bernier, G., Andrejewski, N., Kammandel, B., Wagner, M., and Gruss, P. (2000). Spatial specification of mammalian eye territories by reciprocal transcriptional repression of Pax2 and Pax6. Development *127*, 4325-4334.
19. Shimamura, K., and Rubenstein, J.L. (1997). Inductive interactions direct early regionalization of the mouse forebrain. Development *124*, 2709-2718.
20. Storm, E.E., Garel, S., Borello, U., Hebert, J.M., Martinez, S., McConnell, S.K., Martin, G.R., and Rubenstein, J.L. (2006). Dose-dependent functions of Fgf8 in regulating telencephalic patterning centers. Development *133*, 1831-1844. 133/9/1831 [pii] 10.1242/dev.02324.
21. Soukkarieh, C., Agius, E., Soula, C., and Cochard, P. (2007). Pax2 regulates neuronal-glial cell fate choice in the embryonic optic nerve. Dev Biol *303*, 800-813. 10.1016/j.ydbio.2006.11.016.
22. Martinez-Morales, J.R., Del Bene, F., Nica, G., Hammerschmidt, M., Bovolenta, P., and Wittbrodt, J. (2005). Differentiation of the vertebrate retina is coordinated by an FGF signaling center. Developmental cell *8*, 565-574. 10.1016/j.devcel.2005.01.022.
23. Vogel-Hopker, A., Momose, T., Rohrer, H., Yasuda, K., Ishihara, L., and Rapaport, D.H. (2000). Multiple functions of fibroblast growth factor-8 (FGF-8) in chick eye development. Mech Dev *94*, 25-36. 10.1016/s0925-4773(00)00320-8.
24. Lancaster, M.A., and Knoblich, J.A. (2014). Organogenesis in a dish: modeling development and disease using organoid technologies. Science *345*, 1247125. 10.1126/science.1247125.
25. Eiraku, M., Takata, N., Ishibashi, H., Kawada, M., Sakakura, E., Okuda, S., Sekiguchi, K., Adachi, T., and Sasai, Y. (2011). Self-organizing optic-cup morphogenesis in three-dimensional culture. Nature *472*, 51-56. 10.1038/nature09941.
26. Meyer, J.S., Howden, S.E., Wallace, K.A., Verhoeven, A.D., Wright, L.S., Capowski, E.E., Pinilla, I., Martin, J.M., Tian, S., Stewart, R., et al. (2011). Optic vesicle-like structures derived from human pluripotent stem cells facilitate a customized approach to retinal disease treatment. Stem Cells *29*, 1206-1218. 10.1002/stem.674.
27. Nakano, T., Ando, S., Takata, N., Kawada, M., Muguruma, K., Sekiguchi, K., Saito, K., Yonemura, S., Eiraku, M., and Sasai, Y. (2012). Self-formation of optic cups and storable stratified neural retina from human ESCs. Cell Stem Cell *10*, 771-785. 10.1016/j.stem.2012.05.009.
28. Lowe, A., Harris, R., Bhansali, P., Cvekl, A., and Liu, W. (2016). Intercellular Adhesion-Dependent Cell Survival and ROCK-Regulated Actomyosin-Driven Forces Mediate Self-Formation of a Retinal Organoid. Stem Cell Reports *6*, 743-756. 10.1016/j.stemcr.2016.03.011.
29. Zhong, X., Gutierrez, C., Xue, T., Hampton, C., Vergara, M.N., Cao, L.H., Peters, A., Park, T.S., Zambidis, E.T., Meyer, J.S., et al. (2014). Generation of three-dimensional

retinal tissue with functional photoreceptors from human iPSCs. Nature communications *5*, 4047. 10.1038/ncomms5047.

30. Reichman, S., Terray, A., Slembrouck, A., Nanteau, C., Orieux, G., Habeler, W., Nandrot, E.F., Sahel, J.A., Monville, C., and Goureau, O. (2014). From confluent human iPS cells to self-forming neural retina and retinal pigmented epithelium. Proc Natl Acad Sci U S A *111*, 8518-8523. 10.1073/pnas.1324212111.

31. Cowan, C.S., Renner, M., De Gennaro, M., Gross-Scherf, B., Goldblum, D., Hou, Y., Munz, M., Rodrigues, T.M., Krol, J., Szikra, T., et al. (2020). Cell Types of the Human Retina and Its Organoids at Single-Cell Resolution. Cell *182*, 1623-1640 e1634. 10.1016/j.cell.2020.08.013.

32. Fligor, C.M., Lavekar, S.S., Harkin, J., Shields, P.K., VanderWall, K.B., Huang, K.C., Gomes, C., and Meyer, J.S. (2021). Extension of retinofugal projections in an assembled model of human pluripotent stem cell-derived organoids. Stem Cell Reports. 10.1016/j.stemcr.2021.05.009.

33. Kim, S., Lowe, A., Dharmat, R., Lee, S., Owen, L.A., Wang, J., Shakoor, A., Li, Y., Morgan, D.J., Hejazi, A.A., et al. (2019). Generation, transcriptome profiling, and functional validation of cone-rich human retinal organoids. Proc Natl Acad Sci U S A *116*, 10824-10833. 10.1073/pnas.1901572116.

34. Langer, K.B., Ohlemacher, S.K., Phillips, M.J., Fligor, C.M., Jiang, P., Gamm, D.M., and Meyer, J.S. (2018). Retinal Ganglion Cell Diversity and Subtype Specification from Human Pluripotent Stem Cells. Stem Cell Reports *10*, 1282-1293. 10.1016/j.stemcr.2018.02.010.

35. Fligor, C.M., Langer, K.B., Sridhar, A., Ren, Y., Shields, P.K., Edler, M.C., Ohlemacher, S.K., Sluch, V.M., Zack, D.J., Zhang, C., et al. (2018). Three-Dimensional Retinal Organoids Facilitate the Investigation of Retinal Ganglion Cell Development, Organization and Neurite Outgrowth from Human Pluripotent Stem Cells. Sci Rep *8*, 14520. 10.1038/s41598-018-32871-8.

36. Teotia, P., Chopra, D.A., Dravid, S.M., Van Hook, M.J., Qiu, F., Morrison, J., Rizzino, A., and Ahmad, I. (2017). Generation of Functional Human Retinal Ganglion Cells with Target Specificity from Pluripotent Stem Cells by Chemically Defined Recapitulation of Developmental Mechanism. Stem Cells *35*, 572-585. 10.1002/stem.2513.

37. Lancaster, M.A., Renner, M., Martin, C.A., Wenzel, D., Bicknell, L.S., Hurles, M.E., Homfray, T., Penninger, J.M., Jackson, A.P., and Knoblich, J.A. (2013). Cerebral organoids model human brain development and microcephaly. Nature *501*, 373-379. 10.1038/nature12517.

38. Kadoshima, T., Sakaguchi, H., Nakano, T., Soen, M., Ando, S., Eiraku, M., and Sasai, Y. (2013). Self-organization of axial polarity, inside-out layer pattern, and species-specific progenitor dynamics in human ES cell-derived neocortex. Proc Natl Acad Sci U S A *110*, 20284-20289. 10.1073/pnas.1315710110.

39. Mariani, J., Simonini, M.V., Palejev, D., Tomasini, L., Coppola, G., Szekely, A.M., Horvath, T.L., and Vaccarino, F.M. (2012). Modeling human cortical development in vitro using induced pluripotent stem cells. Proc Natl Acad Sci U S A *109*, 12770-12775. 10.1073/pnas.1202944109.

40. Qian, X., Nguyen, H.N., Jacob, F., Song, H., and Ming, G.L. (2017). Using brain organoids to understand Zika virus-induced microcephaly. Development *144*, 952-957. 10.1242/dev.140707.

41. Velasco, S., Kedaigle, A.J., Simmons, S.K., Nash, A., Rocha, M., Quadrato, G., Paulsen, B., Nguyen, L., Adiconis, X., Regev, A., et al. (2019). Individual brain organoids reproducibly form cell diversity of the human cerebral cortex. Nature *570*, 523-527. 10.1038/s41586-019-1289-x.
42. Gabriel, E., Albanna, W., Pasquini, G., Ramani, A., Josipovic, N., Mariappan, A., Schinzel, F., Karch, C.M., Bao, G., Gottardo, M., et al. (2021). Human brain organoids assemble functionally integrated bilateral optic vesicles. Cell Stem Cell. 10.1016/j.stem.2021.07.010.
43. Etoc, F., Metzger, J., Ruzo, A., Kirst, C., Yoney, A., Ozair, M.Z., Brivanlou, A.H., and Siggia, E.D. (2016). A Balance between Secreted Inhibitors and Edge Sensing Controls Gastruloid Self-Organization. Developmental cell *39*, 302-315. 10.1016/j.devcel.2016.09.016.
44. Minn, K.T., Fu, Y.C., He, S., Dietmann, S., George, S.C., Anastasio, M.A., Morris, S.A., and Solnica-Krezel, L. (2020). High-resolution transcriptional and morphogenetic profiling of cells from micropatterned human ESC gastruloid cultures. Elife *9*. 10.7554/eLife.59445.
45. Xue, X., Sun, Y., Resto-Irizarry, A.M., Yuan, Y., Aw Yong, K.M., Zheng, Y., Weng, S., Shao, Y., Chai, Y., Studer, L., and Fu, J. (2018). Mechanics-guided embryonic patterning of neuroectoderm tissue from human pluripotent stem cells. Nat Mater *17*, 633-641. 10.1038/s41563-018-0082-9.
46. Hayashi, R., Ishikawa, Y., Sasamoto, Y., Katori, R., Nomura, N., Ichikawa, T., Araki, S., Soma, T., Kawasaki, S., Sekiguchi, K., et al. (2016). Co-ordinated ocular development from human iPS cells and recovery of corneal function. Nature *531*, 376-380. 10.1038/nature17000.
47. Zhu, Y., Carido, M., Meinhardt, A., Kurth, T., Karl, M.O., Ader, M., and Tanaka, E.M. (2013). Three-dimensional neuroepithelial culture from human embryonic stem cells and its use for quantitative conversion to retinal pigment epithelium. PLoS One *8*, e54552. 10.1371/journal.pone.0054552.
48. Suda, Y., Kokura, K., Kimura, J., Kajikawa, E., Inoue, F., and Aizawa, S. (2010). The same enhancer regulates the earliest Emx2 expression in caudal forebrain primordium, subsequent expression in dorsal telencephalon and later expression in the cortical ventricular zone. Development *137*, 2939-2949. 10.1242/dev.048843.
49. Danesh, S.M., Villasenor, A., Chong, D., Soukup, C., and Cleaver, O. (2009). BMP and BMP receptor expression during murine organogenesis. Gene Expr Patterns *9*, 255-265. 10.1016/j.gep.2009.04.002.
50. Furuta, Y., and Hogan, B.L. (1998). BMP4 is essential for lens induction in the mouse embryo. Genes Dev *12*, 3764-3775. 10.1101/gad.12.23.3764.
51. Dudley, A.T., and Robertson, E.J. (1997). Overlapping expression domains of bone morphogenetic protein family members potentially account for limited tissue defects in BMP7 deficient embryos. Dev Dyn *208*, 349-362. 10.1002/(SICI)1097-0177(199703)208:3<349::AID-AJA6>3.0.CO;2-I.
52. Solloway, M.J., Dudley, A.T., Bikoff, E.K., Lyons, K.M., Hogan, B.L., and Robertson, E.J. (1998). Mice lacking Bmp6 function. Dev Genet *22*, 321-339. 10.1002/(SICI)1520-6408(1998)22:4<321::AID-DVG3>3.0.CO;2-8.

53. Morcillo, J., Martinez-Morales, J.R., Trousse, F., Fermin, Y., Sowden, J.C., and Bovolenta, P. (2006). Proper patterning of the optic fissure requires the sequential activity of BMP7 and SHH. Development *133*, 3179-3190. 10.1242/dev.02493.
54. Gan, L., Xiang, M., Zhou, L., Wagner, D.S., Klein, W.H., and Nathans, J. (1996). POU domain factor Brn-3b is required for the development of a large set of retinal ganglion cells. Proc Natl Acad Sci U S A *93*, 3920-3925.
55. Mui, S.H., Kim, J.W., Lemke, G., and Bertuzzi, S. (2005). Vax genes ventralize the embryonic eye. Genes Dev *19*, 1249-1259. 10.1101/gad.1276605.
56. Bassett, E.A., Williams, T., Zacharias, A.L., Gage, P.J., Fuhrmann, S., and West-Mays, J.A. (2010). AP-2alpha knockout mice exhibit optic cup patterning defects and failure of optic stalk morphogenesis. Hum Mol Genet *19*, 1791-1804. 10.1093/hmg/ddq060.
57. Biswas, S.K., Lee, J.E., Brako, L., Jiang, J.X., and Lo, W.K. (2010). Gap junctions are selectively associated with interlocking ball-and-sockets but not protrusions in the lens. Mol Vis *16*, 2328-2341.
58. Lovicu, F.J., and McAvoy, J.W. (2001). FGF-induced lens cell proliferation and differentiation is dependent on MAPK (ERK1/2) signalling. Development *128*, 5075-5084.
59. Stuart, T., Butler, A., Hoffman, P., Hafemeister, C., Papalexi, E., Mauck, W.M., 3rd, Hao, Y., Stoeckius, M., Smibert, P., and Satija, R. (2019). Comprehensive Integration of Single-Cell Data. Cell *177*, 1888-1902 e1821. 10.1016/j.cell.2019.05.031.
60. Tirosh, I., Izar, B., Prakadan, S.M., Wadsworth, M.H., 2nd, Treacy, D., Trombetta, J.J., Rotem, A., Rodman, C., Lian, C., Murphy, G., et al. (2016). Dissecting the multicellular ecosystem of metastatic melanoma by single-cell RNA-seq. Science *352*, 189-196. 10.1126/science.aad0501.
61. Yao, Z., Mich, J.K., Ku, S., Menon, V., Krostag, A.R., Martinez, R.A., Furchtgott, L., Mulholland, H., Bort, S., Fuqua, M.A., et al. (2017). A Single-Cell Roadmap of Lineage Bifurcation in Human ESC Models of Embryonic Brain Development. Cell Stem Cell *20*, 120-134. 10.1016/j.stem.2016.09.011.
62. Poh, Y.C., Chen, J., Hong, Y., Yi, H., Zhang, S., Chen, J., Wu, D.C., Wang, L., Jia, Q., Singh, R., et al. (2014). Generation of organized germ layers from a single mouse embryonic stem cell. Nat Commun *5*, 4000. 10.1038/ncomms5000.
63. Varga, B.V., Faiz, M., Yang, H., Pivonkova, H., Gao, S., Khelifi, G., Linderoth, E., Zhen, M., Hussein, S.M., and Nagy, A. (2021). Signal requirement for cortical potential of transplantable human neuroepithelial stem cells. biorxiv *https://doi.org/10.1101/2021.03.27.437311*. https://doi.org/10.1101/2021.03.27.437311.
64. Simoes-Costa, M., and Bronner, M.E. (2015). Establishing neural crest identity: a gene regulatory recipe. Development *142*, 242-257. 10.1242/dev.105445.
65. Chatterjee, M., and Li, J.Y. (2012). Patterning and compartment formation in the diencephalon. Front Neurosci *6*, 66. 10.3389/fnins.2012.00066.
66. Martinez-Ferre, A., and Martinez, S. (2012). Molecular regionalization of the diencephalon. Front Neurosci *6*, 73. 10.3389/fnins.2012.00073.
67. Oster, S.F., Bodeker, M.O., He, F., and Sretavan, D.W. (2003). Invariant Sema5A inhibition serves an ensheathing function during optic nerve development. Development *130*, 775-784. 10.1242/dev.00299.
68. Sandberg-Lall, M., Hagg, P.O., Wahlstrom, I., and Pihlajaniemi, T. (2000). Type XIII collagen is widely expressed in the adult and developing human eye and accentuated in

the ciliary muscle, the optic nerve and the neural retina. Exp Eye Res *70*, 401-410. 10.1006/exer.1998.0826.

69. Chatzopoulou, E., Miguez, A., Savvaki, M., Levasseur, G., Muzerelle, A., Muriel, M.P., Goureau, O., Watanabe, K., Goutebroze, L., Gaspar, P., et al. (2008). Structural requirement of TAG-1 for retinal ganglion cell axons and myelin in the mouse optic nerve. J Neurosci *28*, 7624-7636. 10.1523/JNEUROSCI.1103-08.2008.

70. Yamagata, M., and Sanes, J.R. (2012). Expanding the Ig superfamily code for laminar specificity in retina: expression and role of contactins. J Neurosci *32*, 14402-14414. 10.1523/JNEUROSCI.3193-12.2012.

71. Li, H., Wagner, E., McCaffery, P., Smith, D., Andreadis, A., and Drager, U.C. (2000). A retinoic acid synthesizing enzyme in ventral retina and telencephalon of the embryonic mouse. Mech Dev *95*, 283-289. 10.1016/s0925-4773(00)00352-x.

72. Take-uchi, M., Clarke, J.D., and Wilson, S.W. (2003). Hedgehog signalling maintains the optic stalk-retinal interface through the regulation of Vax gene activity. Development *130*, 955-968. 10.1242/dev.00305.

73. Bedzhov, I., and Zernicka-Goetz, M. (2014). Self-organizing properties of mouse pluripotent cells initiate morphogenesis upon implantation. Cell *156*, 1032-1044. 10.1016/j.cell.2014.01.023.

74. Coucouvanis, E., and Martin, G.R. (1995). Signals for death and survival: a two-step mechanism for cavitation in the vertebrate embryo. Cell *83*, 279-287.

75. Chambers, S.M., Fasano, C.A., Papapetrou, E.P., Tomishima, M., Sadelain, M., and Studer, L. (2009). Highly efficient neural conversion of human ES and iPS cells by dual inhibition of SMAD signaling. Nat Biotechnol *27*, 275-280. 10.1038/nbt.1529.

76. Fernando, M., Lee, S., Wark, J.R., Xiao, D., Lim, B.Y., O'Hara-Wright, M., Kim, H.J., Smith, G.C., Wong, T., Teber, E.T., et al. (2022). Differentiation of brain and retinal organoids from confluent cultures of pluripotent stem cells connected by nerve-like axonal projections of optic origin. Stem Cell Reports *17*, 1476-1492. 10.1016/j.stemcr.2022.04.003.

77. Argelaguet, R., Clark, S.J., Mohammed, H., Stapel, L.C., Krueger, C., Kapourani, C.A., Imaz-Rosshandler, I., Lohoff, T., Xiang, Y., Hanna, C.W., et al. (2019). Multi-omics profiling of mouse gastrulation at single-cell resolution. Nature *576*, 487-491. 10.1038/s41586-019-1825-8.

78. Tropepe, V., Hitoshi, S., Sirard, C., Mak, T.W., Rossant, J., and van der Kooy, D. (2001). Direct neural fate specification from embryonic stem cells: a primitive mammalian neural stem cell stage acquired through a default mechanism. Neuron *30*, 65-78. 10.1016/s0896-6273(01)00263-x.

79. Munoz-Sanjuan, I., and Brivanlou, A.H. (2002). Neural induction, the default model and embryonic stem cells. Nat Rev Neurosci *3*, 271-280. 10.1038/nrn786.

80. Redies, C., and Puelles, L. (2001). Modularity in vertebrate brain development and evolution. Bioessays *23*, 1100-1111. 10.1002/bies.10014.

81. Martinez-Morales, J.R., Rodrigo, I., and Bovolenta, P. (2004). Eye development: a view from the retina pigmented epithelium. Bioessays *26*, 766-777. 10.1002/bies.20064.

82. Kuwahara, A., Ozone, C., Nakano, T., Saito, K., Eiraku, M., and Sasai, Y. (2015). Generation of a ciliary margin-like stem cell niche from self-organizing human retinal tissue. Nature communications *6*, 6286. 10.1038/ncomms7286.

885 83. Shirasaki, R., Lewcock, J.W., Lettieri, K., and Pfaff, S.L. (2006). FGF as a target-derived
886 chemoattractant for developing motor axons genetically programmed by the LIM code.
887 Neuron *50*, 841-853. 10.1016/j.neuron.2006.04.030.
888 84. Sluch, V.M., Chamling, X., Liu, M.M., Berlinicke, C.A., Cheng, J., Mitchell, K.L.,
889 Welsbie, D.S., and Zack, D.J. (2017). Enhanced Stem Cell Differentiation and
890 Immunopurification of Genome Engineered Human Retinal Ganglion Cells. Stem Cells
891 Transl Med *6*, 1972-1986. 10.1002/sctm.17-0059.
892 85. Rabesandratana, O., Chaffiol, A., Mialot, A., Slembrouck-Brec, A., Joffrois, C., Nanteau,
893 C., Rodrigues, A., Gagliardi, G., Reichman, S., Sahel, J.A., et al. (2020). Generation of a
894 Transplantable Population of Human iPSC-Derived Retinal Ganglion Cells. Front Cell
895 Dev Biol *8*, 585675. 10.3389/fcell.2020.585675.
896 86. Visel, A., Thaller, C., and Eichele, G. (2004). GenePaint.org: an atlas of gene expression
897 patterns in the mouse embryo. Nucleic Acids Res *32*, D552-556. 10.1093/nar/gkh029.
898

899

900 **Figure legends**

901 **Figure 1. Generation of a telencephalon-eye organoid composed of concentric zones of**
902 **anterior ectodermal progenitors (CONCEPT). (A)** A scheme of the procedure. **(B)** A diagram
903 of CONCEPT organoids showing concentric zones of the anterior ectodermal progenitors. See
904 also Figs.1, 2, 3, 5, S1, S10. **(C)** Morphology of cysts at day 2 showing the epithelial structure
905 indicated by the apical reporter TJ::GFP at the lumen. **(D)** Morphology of CONCEPT organoids
906 at day 26. **(E-G)** Expression of telencephalon (Tel) marker Foxg1, neuroretinal (NR) markers
907 Vsx2 and Pax6 in mouse eyes at E10-10.5. Rostral optic stalk (OS) connected the telencephalic
908 vesicle to the optic cup. **(H-O)** FOXG1+ telencephalic progenitors, VSX2+ and/or PAX6+ retinal
909 progenitors formed concentric zones in CONCEPT organoids. N > 5 experiments. **(P-W)** In
910 CONCEPT organoids, morphogens FGF8, BMP4, and BMP7 mRNA expression started at early
911 stages and subsequently formed circular gradients. N > 5 experiments. Scale bars, 100 μm (C,
912 E, M, O, P, S, T), 200 μm (I, K), 500 μm (Q, U), 1 mm (D, H, J, L, N, R, V, W).

913 **Fig. 2. Retinal ganglion cells (RGCs) grow axons toward and then along a path defined by**
914 **PAX2+ cell populations in CONCEPT telencephalon-eye organoids.** N > 5 experiments. **(A-**
915 **D)** POU4F2+ RGCs grew TUBB3+ axons toward and then along a path with a circular or a
916 portion of circular shape. **(E, F)** In mice, Pax2 was expressed in central regions of the retina and
917 optic stalk at E10.5 (E) and in the optic disc and optic stalk at E13.5 (F). Tubb3+ axons from the
918 initial RGCs grew toward the optic disc, exited the eye, and navigated within the optic stalk (G).
919 **(H-L)** In CONCEPT organoids at day 26, TUBB3+ RGC axons grew toward and then along a
920 path defined by an adjacent PAX2+ VSX2+ cell population (arrowhead in H, brackets in I, J); the
921 PAX2+ VSX2- cell population sets up an inner boundary of RGC axon growth. **(L)** A diagram
922 summarizing RGC axon growth, PAX2+ optic disc (OD), and PAX2+ optic stalk (OS) in
923 CONCEPT organoids. The area labeled by the asterisk may appear as false signals in a low-
924 resolution printout but it is clearly a background in digital display. **(M)** A count of CONCEPT

925 organoids showing directional retinal ganglion cell axons. Scale bars, 50 μm (E, F, G), 100 μm
926 (B), 200 μm (A, H, I).

927 **Fig. 3. CONCEPT telencephalon-eye organoids contain lens cells that undergo terminal**
928 **differentiation.** N > 5 experiments. **(A-H)** In CONCEPT organoids, lens markers CRYAA and
929 CRY B were expressed at day 22 (A, B) and day 39 (C, D). Lens cells were not stained by DAPI
930 (E, F); they exhibited a crystal-like shape (G). A count of CONCEPT organoids with these lens
931 cells is shown (H). **(I, J)** When CONCEPT organoids were detached using Dispase at around
932 day 28 and grown in suspension, crystal-like clusters were found (I) and survived for months (J).
933 **(K-L)** Crystal-like lens clusters were free of organelles and exhibited ball-and-socket structures
934 (K, L), as revealed by electron microscopy. Scale bars, 100 μm (A, B, C, D, I), 200 μm (J), 5 μm
935 (K), 200 nm (L).

936 **Fig. 4. Cell clustering analysis identifies telencephalic cells, ocular cells, and two PAX2+**
937 **cell populations that mimic the optic disc and optic stalk, respectively.** See also suppl.
938 Figs. S2-S8. CONCEPT organoids at day 24 were used for single-cell RNA sequencing and
939 analyzed using Seurat (v3.2.0). **(A)** Identification of 14 cell clusters. **(B)** Cell cycle phases as
940 shown as cell cycle scores. **(C)** FOXG1 expression marked telencephalic cells. **(D, E)** The
941 expression of PAX6 and/or VSX2 marked retinal cells. **(F)** PAX2+ cells were found in two major
942 cell populations: PAX2+ VSX2+ cells were assigned as the optic disc (OD), whereas PAX2+
943 FOXG1+ VSX2- cells were assigned as the optic stalk (OS). **(G)** The expression of the optic
944 disc/stalk marker SEMA5A. **(H-L)** The expression of major DEGs in cluster 2, the major cell
945 population that mimic the optic disc. **(M-P)** The expression of major gene markers for PAX2+
946 VSX2- optic stalk cells. **(Q-T)** Identification of glycosylphosphatidylinositol (GPI)-anchored cell
947 membrane protein CNTN2 as a specific marker for developing human RGCs. Cluster 11
948 differentially expressed RGC markers, including CNTN2.

949 **Fig. 5. RGCs grow CNTN2+ axons toward and then along a defined path in CONCEPT**
950 **telencephalon-eye organoids and can be isolated in one step via CNTN2 in a native**
951 **condition.** N > 5 experiments. **(A-F)** PAX2+ cells formed two concentric zones mimicking the
952 optic stalk (OS) and optic disc (OD), respectively (A-C; high magnifications in D, E). POU4F2+
953 RGCs grew CNTN2+ axons toward and then along a path defined by adjacent PAX2+ optic-disc
954 cells (A-E). RGCs at a few hundreds of micrometers away from PAX2+ optic-disc cells grew
955 axons centrifugally (arrow in C). At regions where there was a gap in PAX2+ optic-disc cells,
956 CNTN2+ RGC axons exited the circular path and grew centrifugally (diamond arrowhead in A,
957 double arrowheads in B and F). PAX2+ optic-stalk cells set up an inner boundary for RGC axon
958 growth. **(G, H)** PAX2+ optic-disc cells did not express ALDH1A3; the cells that set up the
959 boundaries of the path highly expressed ALDH1A3. **(I, J)** Cells that set up the inner boundary
960 for RGC axon growth expressed VAX1/VAX2. **(K)** In E13.5 mouse eye, Aldh1a3 was highly
961 expressed in the peripheral retina and a small region in the optic disc. Aldh1a3 expression was
962 at low or nearly absent in the central retina. **(L-P)** One-step isolation of RGCs. RGCs from
963 floating retinal organoids at day 41 (L, M) and day 70 (N-O) were dissociated into single cells
964 using Accutase and then isolated using MACS via CNTN2 for 10-day growth. Isolated RGCs
965 expressed POU4F2 and grew TUBB3+ neurites in random directions (L). RGCs also expressed
966 CNTN2 (M), ISL1 (N), RBPMS (N), and SNCG (O); positive cells were counted (P). Scale bars,
967 200 μm (A,G,I), 100 μm (D-F,H,J,K), 50 μm (L).

968 **Fig. 6. Electrophysiological features of RGCs**. RGCs from retinal organoids on day 48 were
969 isolated using MACS via a CNTN2 antibody and then grown on polymer coverslips in a chamber
970 slide for 20-25 days before whole-cell patch clamp recordings. **(A)** Resting membrane potential
971 of RGCs. *Black triangle: average; black line: median; box: interquartile range, n=9*. **(B)** RGCs
972 can fire action potentials. Cells were patched in current-clamp mode. A steady current (I_m) was
973 injected to maintain the membrane potential at -70mV and depolarizing current steps of 10ms

(*left*), 100ms (*middle*) or 1s (*right*) were injected to elicit action potentials (V_m). **(C)** RGCs show functional voltage-gated currents. Cells were recorded in voltage-clamp (holding=-80mV) and depolarizing voltage steps (200ms, +10mV steps up to 80mV, V_m) were applied to record inward and outward voltage-gated currents (I_m). *Inset*: zoom on inward currents. **(D)** Outward currents are primarily due to voltage-gated potassium channels. *Left*, representative example of a current-voltage experiment performed in presence of 20mM Tetraethylammonium (TEA), a blocker of voltage-gated potassium channels. *Inset*: zoom on inward currents. *Right*, amplitude of potassium current as a function of membrane potential (*mean±SEM;* $n_{control}=5$, $n_{TEA}=5$). **(E)** Inward currents result from activity of voltage-gated sodium channels. *Left*, representative example of a current-voltage experiment performed in presence of 1μM Tetrodotoxin (TTX), a blocker of voltage-gated sodium channels. *Inset*: zoom on inward currents. *Right*, amplitude of sodium current as a function of membrane potential (*mean±SEM;* $n_{control}=5$, $n_{TTX}=3$).

Fig. 7. FGF signaling mediated by FGFRs is required for early RGC differentiation and directional axon growth. (A) PAX2, FGF9, and FGF8 are differentially expressed in cluster 2, the major component of PAX2+ optic-disc cells. **(B)** PAX2 mRNA expression in CONCEPT organoids on day 25. Two PAX2+ concentric zones corresponding to the optic stalk (OS) and optic disc (OD) are labeled. **(C)** Dual-color immunocytochemistry indicates the co-localization of FGF8 and PAX2 in the optic-disc zone of CONCEPT organoids on day 25. **(D-E)** TUBB3+ axons grew towards and then along the cells that expressed high levels of FGF8 (D) and FGF9 mRNA (E) in CONCEPT organoids on day 25. Immunocytochemistry of TUBB3 was performed after in situ hybridization. **(F-K)** After the inhibition of FGF signaling with FGFR inhibitor PD 161570 during days 17-24, the number of RGC somas drastically reduced, and directional axon growth of RGCs was nearly absent, whereas FGF8 protein expression largely remained. CNTN2 immunocytochemistry before (F, H) and after FGF8 immunocytochemistry (G, I, J, K) are shown. N = 3/3 experiments. Scale bar, 250 μm (B), 100 μm (C-E), 1 mm (F), 200 μm (K).

999 **Tab. 1.** Cell counts of clusters in the scRNA-seq dataset.

1000 Abbreviations: Idents, assigned cell identities; # Cells, cell number; Tel, telencephalon; R, retina;
1001 OD, optic disc; OS, optic stalk; RPE, retina pigment epithelium; RGC, retinal ganglion cell; N,
1002 early neurons; UD, undetermined.

1003 **Supplemental Information**

1004 **Immunostaining, antibodies, and light microscopy**

1005 CONCEPT telencephalon-eye organoids were fixed in 4% PFA for 15-30 minutes at room
1006 temperature and processed for immunostaining. These primary antibodies were used: FOXG1
1007 (Abcam, ab18259, 1:500), TUBB3 (Covance MMS-435P, 1:1000), FGF8 (1:500, R&D MAB323),
1008 RBPMS (1:200, PhosphoSolution 1830-RBPMS), ISL1 (1:500, DSHB 40.2D6), SNCG (1:200,
1009 Abcam ab55424), PAX2 (Invitrogen, 716000, 1:200), alpha A crystallin (Santa Cruz sc 22743,
1010 1:500, shown as CRYAA in figure panels), beta crystallin (Santa Cruz sc-22745, 1:100, shown
1011 as CRY B in figure panels), CNTN2 (DSHB 4D7, 1:100), ALDH1A3 (Invitrogen, PA529188,
1012 1:500), VAX1/2 (Santa Cruz sc-98613, 1:200), PAX6 (1:500, Covance PRB-278P), POU4F2
1013 (Santa Cruz, SC-6026, 1:200), SIX3 (1:500, Rockland), and VSX2 (1:500, Millipore AB9016).
1014 Primary antibodies were visualized using Alexa Fluor 488-, 568-, and 647-conjugated secondary
1015 antibodies and imaged using a Zeiss AxioObserver Z1 microscope. When the sample did not fit
1016 in one image, multiple images were stitched to obtain an overview. In dual-color
1017 immunocytochemistry for PAX2 and FGF8, FGF8 was visualized using AP-conjugated anti
1018 mouse secondary antibody (Invitrogen A16038), and PAX2 was detected by biotin-conjugated
1019 anti rabbit secondary antibody (Invitrogen B2770) followed by HRP-conjugated streptavidin
1020 (ThermoScientific 21130). For dual color immunocytochemistry of CNTN2 and FGF8 (both are
1021 mouse antibodies; no working antibodies raised in different species are available),
1022 immunocytochemistry of CNTN2 was performed first and visualized using HRP-conjugated
1023 streptavidin. Then, the samples were fixed in 4% PFA for 15 minutes to avoid antibody crosstalk.
1024 After that, FGF8 antibody was applied and then detected by an AP-conjugated secondary
1025 antibody. Brown and blue colors are well separated in Fig. 5K, indicating that antibody
1026 crosstalks did not exist.

1027 **PCR Primers for in situ hybridization probes**

1028 PCR primers are as follows: BMP4: forward, CGGAAGCTAGGTGAGTGTGG, reverse,
1029 GAGtaatacgactcactatagggGGAAGCCCCTTTCCCAATCA; BMP7: forward, gaggtccctctccattccct,
1030 reverse, GAGtaatacgactcactatagggtgcacccatcagacctccta; FGF8: forward,
1031 GTTGCACTTGCTGGTCCTCT, reverse,
1032 GAGtaatacgactcactatagggTTGAGTTTTGGGTGCCCTAC; PAX2: forward, gctgtctgtgctgtgagagt,
1033 reverse, GAGtaatacgactcactatagggccggggacatttagcaggtt; SEMA5A: forward,
1034 CAGAGGCTCAGGCACAATGA, reverse,
1035 GAGtaatacgactcactatagggTCCGTGTCTACCCAGGACTT; CYP1B1: forward,
1036 cccagcggttcttcatgagt, reverse, GAGtaatacgactcactatagggcacacttggttgcgttagt; LEFTY2: forward,
1037 agccctctaactgaacgtgtg, reverse, GAGtaatacgactcactatagggtcttctgagtatctacattcaattgct; EMX2:
1038 forward, ACCGAGAAAGGGAGAGGGAA, reverse,
1039 GAGtaatacgactcactatagggTCGGCCAATTTCTCCAACCA; FGF9: forward,
1040 GTCCGCTATGAACCTGTGGT, reverse,
1041 GAGtaatacgactcactatagggATAGTCTCGCTTGCCCAAGG; FGF2: forward,
1042 aacaccgaaatgctggaggt, reverse, GAGtaatacgactcactatagggagaccacatgtacacgcca.

1043 **Whole-cell patch clamp recordings of isolated RGCs in culture.**

1044 RGCs were isolated from retinal organoids on day 48 using MACS via a CNTN2 antibody and
1045 then grown on polymer coverslips in chamber slides (ibidi 80826) for 20 – 27 days. At the time
1046 of whole-cell patch clamping recordings, the polymer coverslips carrying RGCs were carefully
1047 cut out with a scalpel blade and then placed in a recording chamber under an upright
1048 microscope (Zeiss Examiner A1), containing artificial cerebrospinal fluid (aCSF) composed of (*in*
1049 *mM*): NaCl (*140*), $MgCl_2$ (*1*), KCl (*5*), $CaCl_2$ (*2*), Hepes (*10*), Glucose (*10*). Osmolarity and pH
1050 were adjusted to 300mOsm and 7.3 respectively. Whole-cell patch-clamp recordings in voltage
1051 and current-clamp mode were obtained at room temperature using an Optopatch amplifier

1052 (Cairn Research, UK) and acquired with WinWCP 5.2 freeware (John Dempster, SIPBS,
1053 University of Strathclyde, UK). Patch pipettes (3-4MΩ when filled with corresponding solution)
1054 were pulled from borosilicate capillaries using a horizontal puller (Sutter P97, USA) and coated
1055 with dental wax to reduce the pipette capacitance. For current clamp recordings, patch pipettes
1056 were filled with a solution containing (*in mM*): K-gluconate (*130*), Na-gluconate (*10*), NaCl (*4*),
1057 Hepes (*10*), Phosphocreatin (*10*), MgATP (*4*), Na_2GTP (*0.3*). Osmolarity and pH were adjusted
1058 at 295mOsm and 7.3 respectively. Resting membrane potential was obtained from averaging
1059 membrane potential recorded for one minute in I=0 mode immediately after breaking the cell
1060 membrane. In current clamp mode, with the cell hyperpolarized to -70 mV, current steps of 100
1061 to 500pA were made to explore whether the cells were excitable. For voltage-clamp recordings,
1062 cells were held at clamped potential of -80mV, and series resistance was monitored and
1063 compensated (>80%). Membrane potentials were corrected for the liquid junction potential,
1064 calculated at +5.4mV *(*https://swharden.com/LJPcalc*)*. Patch pipettes were filled with a solution
1065 containing (*in mM*): KCl (*140*), $MgCl_2$ (*5*), $CaCl_2$ (*2.5*), Hepes (*10*), MgATP (*4*), Na_2GTP (*0.3*).
1066 Osmolarity and pH were adjusted at 295mOsm and 7.3 respectively. A -P/4 subtraction protocol
1067 was used to isolate voltage-gated currents by removing linear leak current and capacitance
1068 artifacts. In all cases, voltage and current recordings were low pass filtered at 3kHz and
1069 digitized at 10-20kHz (Axon Digidata 1550b, Molecular Device, USA). Tetraethylammonium-
1070 chloride (TEA, Sigma-Aldrich, USA) and Tetrodotoxin-citrate (TTX, Fisher Scientific) stocks
1071 were diluted in aCSF to reach 20mM and 1µM respectively. All recordings were analyzed with
1072 WinWcp 5.2 and custom scripts and routines written in Python 3.9. Statistical tests were
1073 performed with corresponding function from *scipy.stats* package (v1.8).

1074

1075

1076 **Legends for supplemental Figures**

1077 **Fig. S1. Reproducibility of CONCEPT telencephalon-eye organoids is demonstrated by**
1078 **consistent gene expression profiles of multiple organoids in whole culture wells.** Related
1079 to Figs. 1, 7. **(A-C)** CONCEPT organoids on day 17 expressed FGF8 (A, n =5/5), BMP4 (B, n =
1080 4/4; the broken colony was not counted since its morphology is not quite clear), and BMP7 (C, n
1081 = 4/4) in concentric zones. **(D-F)** CONCEPT organoids on day 25 expressed FGF8 (D, n = 5/8),
1082 RGC marker CNTN2 (E, n = 5/6), and telencephalon marker EMX2 (F, n = 2/2) in concentric
1083 zones. Scale bars, 1 mm (A-F).

1084 **Fig. S2. Mesoderm, endoderm, and neural crest markers are not expressed in CONCEPT**
1085 **telencephalon-eye organoids at 24.** Related to Fig. 4. The dataset for Fig. 4 is used for
1086 plotting. Expression profiles of mesoderm markers TBXT, GATA2, and HAND1, endoderm
1087 markers GATA1, GATA4, and SOX17, neural crest markers SNAI1, SOX10, FOXD3 are shown.

1088 **Fig. S3. The expression of top DEGs in cluster 0.** Related to Fig. 4. The dataset for Fig. 4 is
1089 used for plotting. Cluster 0 was marked by DEGs that were lowly expressed.

1090 **Fig. S4. Diencephalon markers and midbrain/hindbrain markers are rarely expressed in**
1091 **CONCEPT telencephalon-eye organoids at day 24.** Related to Fig. 4. **(A-F)** Diencephalon
1092 markers GBX2, WNT3, and SOX14, and midbrain/hindbrain markers EN2, PAX7, and TFAP2B
1093 were rarely expressed. The dataset for Fig. 4 is used for plotting. **(G-L)** Expression of the
1094 diencephalon markers and midbrain/hindbrain markers in the E14.5 mouse brain. The images
1095 were downloaded from a public database (https://gp3.mpg.de/) with permission. Image IDs were
1096 shown following gene symbols.

1097 **Fig. S5. DEGs for telencephalic clusters in CONCEPT telencephalon-eye organoids**
1098 **include markers for both the pallium and subpallium.** Related to Fig. 4 and Fig. S6. DEGs

1099 for telencephalic clusters were used for plotting, and expression of their orthologs in E14.5
1100 mouse brain was shown in Fig. S6. **(A-D)** Expression of the DEGs POU3F3, RGMA, EDNRB,
1101 and SOX13, which orthologs are expressed in the pallium of E14.5 mouse brain (see also Fig.
1102 S6B-E). **(E-L)** Expression of the DEGs DLX2, RGS16, DLX1, DLL1, DLX6-AS1, NEFL, DCX,
1103 and RTN1, which orthologs are expressed in the subpallium of E14.5 mouse brain (see Fig.
1104 S6F-M).

1105 **Fig. S6. Mouse orthologs of the telencephalic DEGs are expressed in both the pallium**
1106 **and subpallium of the E14.5 mouse brain.** Related to Fig. 4 and Fig. S5. The images were
1107 downloaded from a public database (https://gp3.mpg.de/) with permission. Image IDs were
1108 shown following gene symbols. **(A)** Expression of Foxg1. **(B-E)** Expression of the genes Pou3f3,
1109 Rgma, Ednrb, and Sox3 in the pallium of E14.5 mouse brain. **(F-M)** Expression of the genes
1110 Dlx2, Rgs16, Dlx1, Dll1, Dlx6os1, Nefl, Dcx, and Rtn1 in the subpallium of E14.5 mouse brain.

1111 **Fig. S7. DEGs in cluster 6 include RPE markers.** Related to Fig. 4. Top DEGs in cluster 6
1112 include RPE markers PMEL, HSD17B2, DCT, and MITF.

1113 **Fig. S8. Mouse orthologs of the markers for Pax2+ optic disc and Pax2+ optic stalk cell**
1114 **clusters in CONCEPT organoids are indeed expressed in the optic disc and optic**
1115 **stalk/nerve, respectively, in E14.5 mouse embryos.** Related to Fig. 4. In situ hybridization
1116 images of the E14.5 mouse brain were downloaded from a public database (https://gp3.mpg.de/)
1117 with permission. Image IDs were shown following gene symbols. **(A-T)** Expression of the gene
1118 markers in E14.5 brain is shown.

1119 **Fig. S9. CONCEPT telencephalon-eye organoids are generated using hiPSC line AICS**
1120 **0023.** Related to Fig. 7. hiPSCs (AICS 0023) were used for the generation of CONCEPT

1121 telencephalon-eye organoids. **(A-D)** POU4F2+ RGCs grew CNTN2+ axons toward and then
1122 along a circular path defined by PAX2+ cell populations. Scale bar, 500 μm (A), 100 μm (B).

1123 **Fig. S10. Expression signatures of cell cluster 2.** Related to Figs. 4, 5. **(A)** A list of top 10
1124 DEGs and additional DEG markers SEMA5A, PAX2, COL13A1, FGF9, and FGF8 in cluster 2
1125 were identified using Seurat analysis. **(B-E)** Expression of PAX2, SEMA5A, CYP1B1, and
1126 LEFTY2 in CONCEPT organoids at day 25 was revealed by in situ hybridization. The PAX2+
1127 optic disc at the outer zone was marked (bracket in B).

1128 **Fig. S11. FGFR1, FGFR2, FGFR3, MAP2K1, and MAP2K2 are expressed in multiple types**
1129 **of cells in CONCEPT organoids.** Related to Fig. 4. In RGCs, FGFR1 and MAP2K2 were
1130 expressed.

Fig. 1

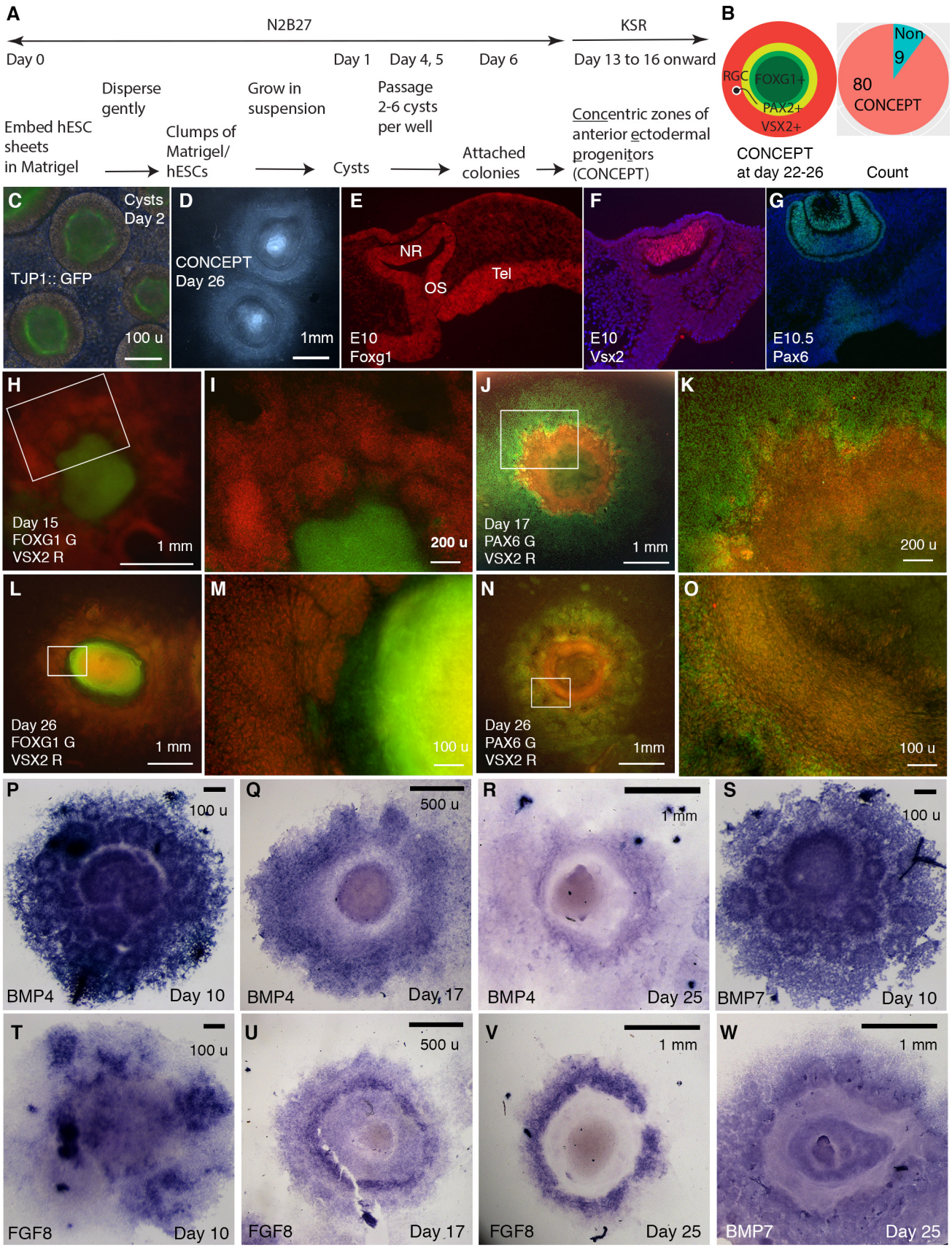
A
N2B27
KSR
Day 0
Day 1
Day 4, 5
Day 6
Day 13 to 16 onward
Embed hESC sheets in Matrigel
Disperse gently
Clumps of Matrigel/ hESCs
Grow in suspension
Cysts
Passage 2-6 cysts per well
Attached colonies
Concentric zones of anterior ectodermal progenitors (CONCEPT)
B
RGC
FOXG1+
PAX2+
VSX2+
CONCEPT at day 22-26
Non
9
80
CONCEPT
Count
C
Cysts Day 2
TJP1:: GFP
100 u
D
CONCEPT Day 26
1mm
E
NR
OS
Tel
E10 Foxg1
F
E10 Vsx2
G
E10.5 Pax6
H
Day 15 FOXG1 G VSX2 R
1 mm
I
200 u
J
Day 17 PAX6 G VSX2 R
1 mm
K
200 u
L
Day 26 FOXG1 G VSX2 R
1 mm
M
100 u
N
Day 26 PAX6 G VSX2 R
1mm
O
100 u
P
100 u
BMP4
Day 10
Q
500 u
BMP4
Day 17
R
1 mm
BMP4
Day 25
S
100 u
BMP7
Day 10
T
100 u
FGF8
Day 10
U
500 u
FGF8
Day 17
V
1 mm
FGF8
Day 25
W
1 mm
BMP7
Day 25

Fig. 2

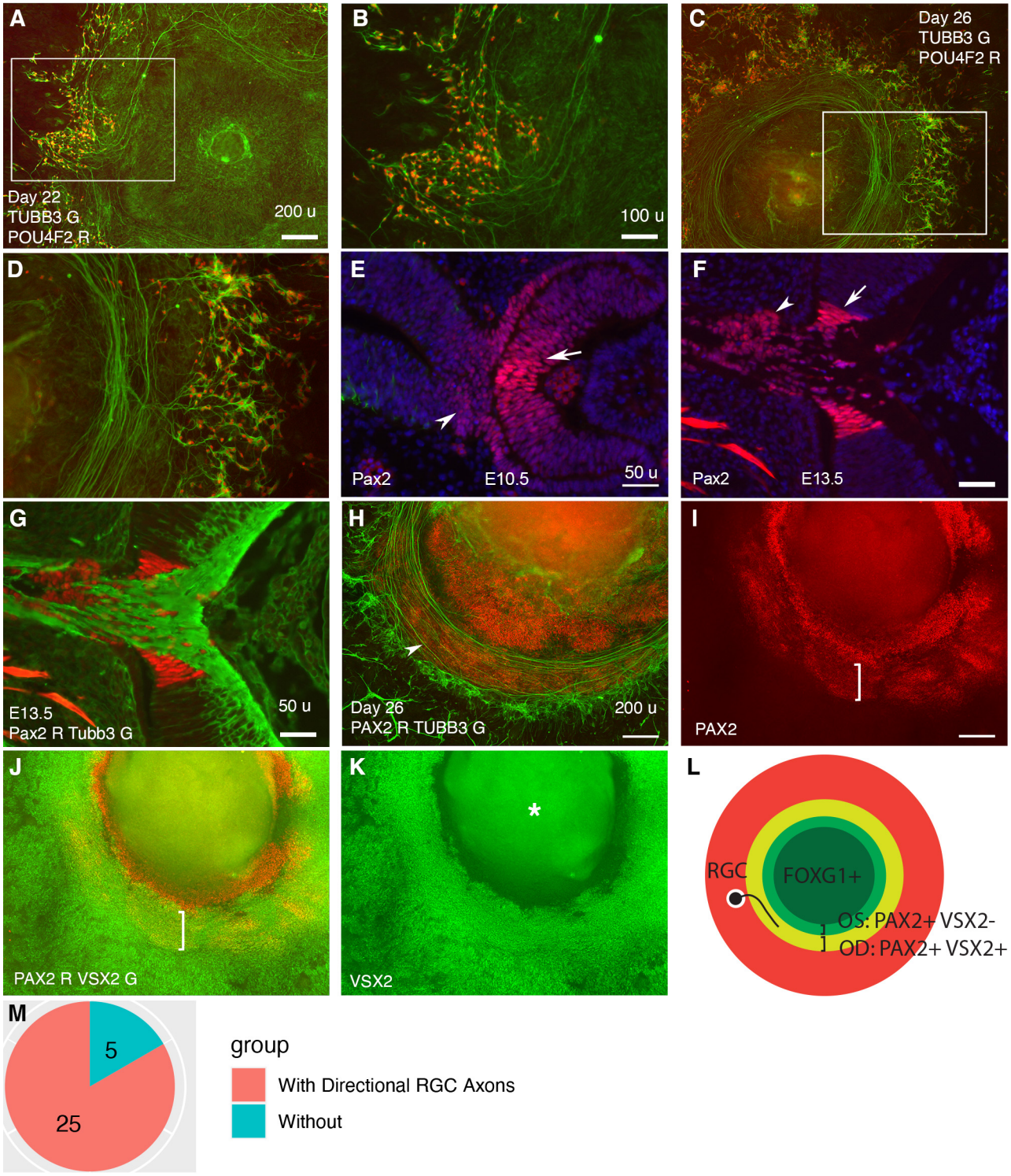
A
Day 22
TUBB3 G
POU4F2 R
200 u
B
100 u
C
Day 26
TUBB3 G
POU4F2 R
D
E
Pax2
E10.5
50 u
F
Pax2
E13.5
G
E13.5
Pax2 R Tubb3 G
50 u
H
Day 26
PAX2 R TUBB3 G
200 u
I
PAX2
J
PAX2 R VSX2 G
K
VSX2
L
RGC
FOXG1+
OS: PAX2+ VSX2-
OD: PAX2+ VSX2+
M
5
25
group
With Directional RGC Axons
Without

Fig. 3

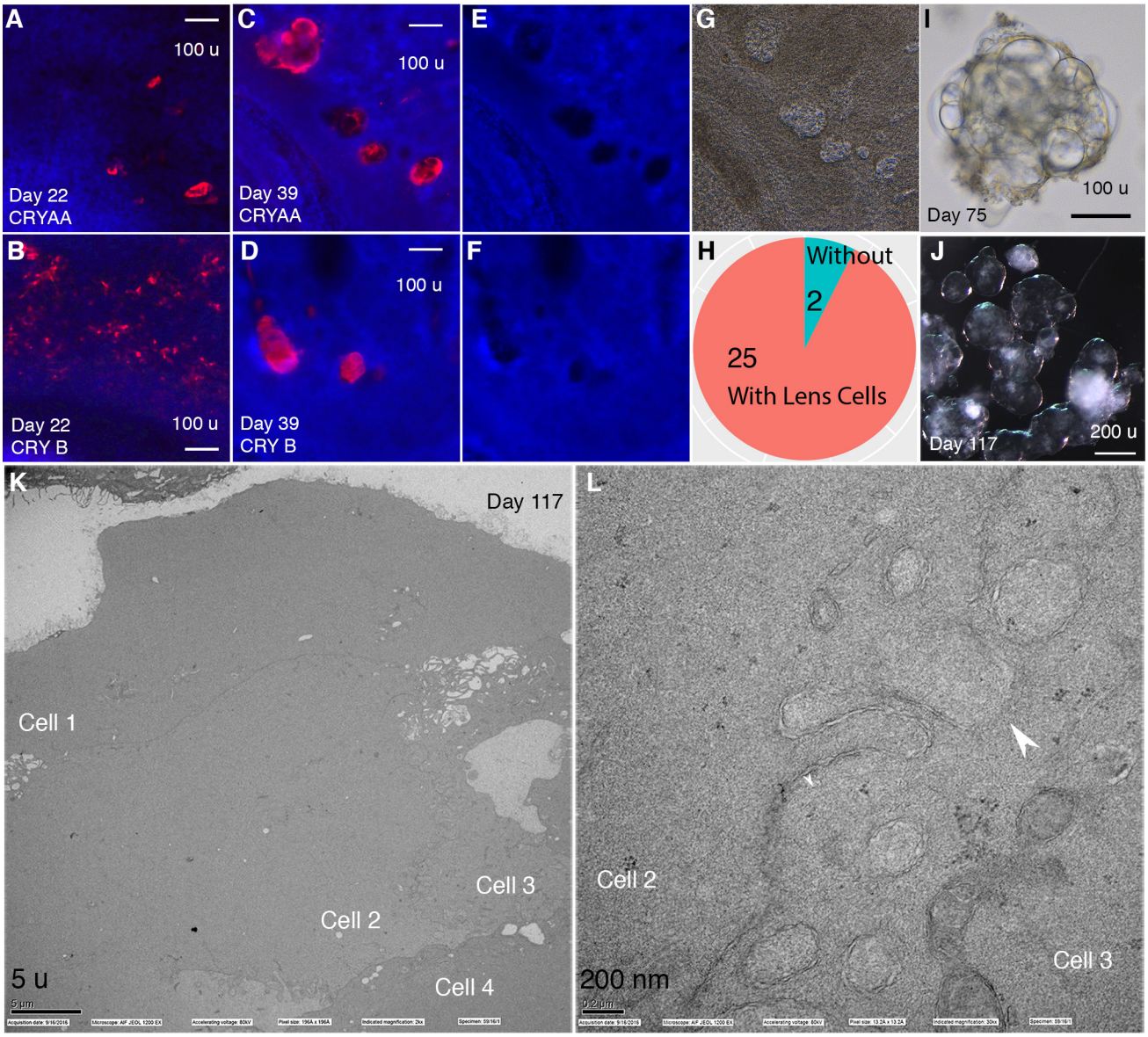
A
100 u
Day 22
CRYAA
C
100 u
Day 39
CRYAA
E
G
I
100 u
Day 75
B
Day 22
CRY B
100 u
D
100 u
Day 39
CRY B
F
H
Without
2
25
With Lens Cells
J
Day 117
200 u
K
Day 117
Cell 1
Cell 3
Cell 2
Cell 4
5 u
L
Cell 2
Cell 3
200 nm

Fig. 4

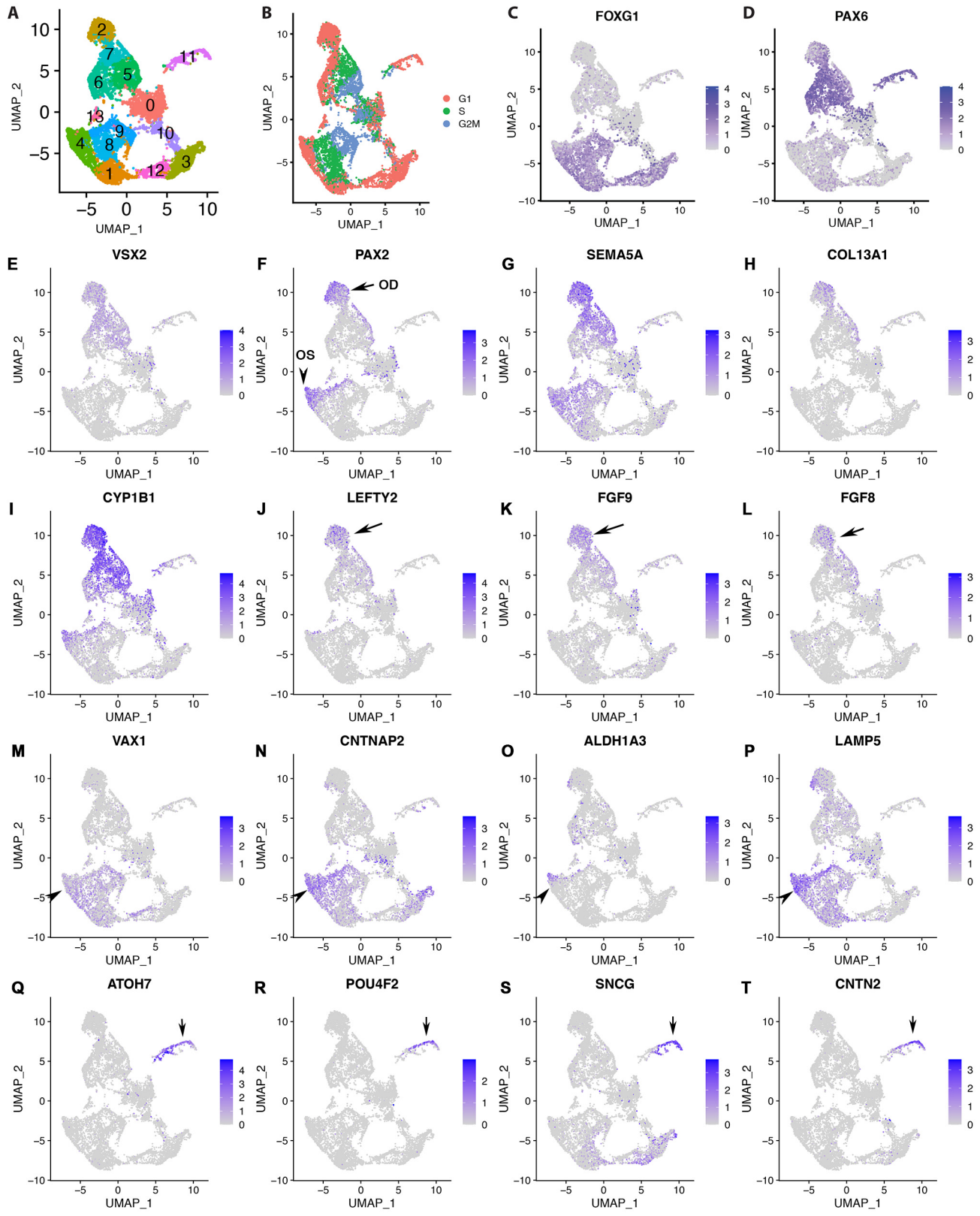
A
B
C
D
E
F
G
H
I
J
K
L
M
N
O
P
Q
R
S
T
UMAP_1
UMAP_2
G1
S
G2M
FOXG1
PAX6
VSX2
PAX2
OD
OS
SEMA5A
COL13A1
CYP1B1
LEFTY2
FGF9
FGF8
VAX1
CNTNAP2
ALDH1A3
LAMP5
ATOH7
POU4F2
SNCG
CNTN2

Fig. 5

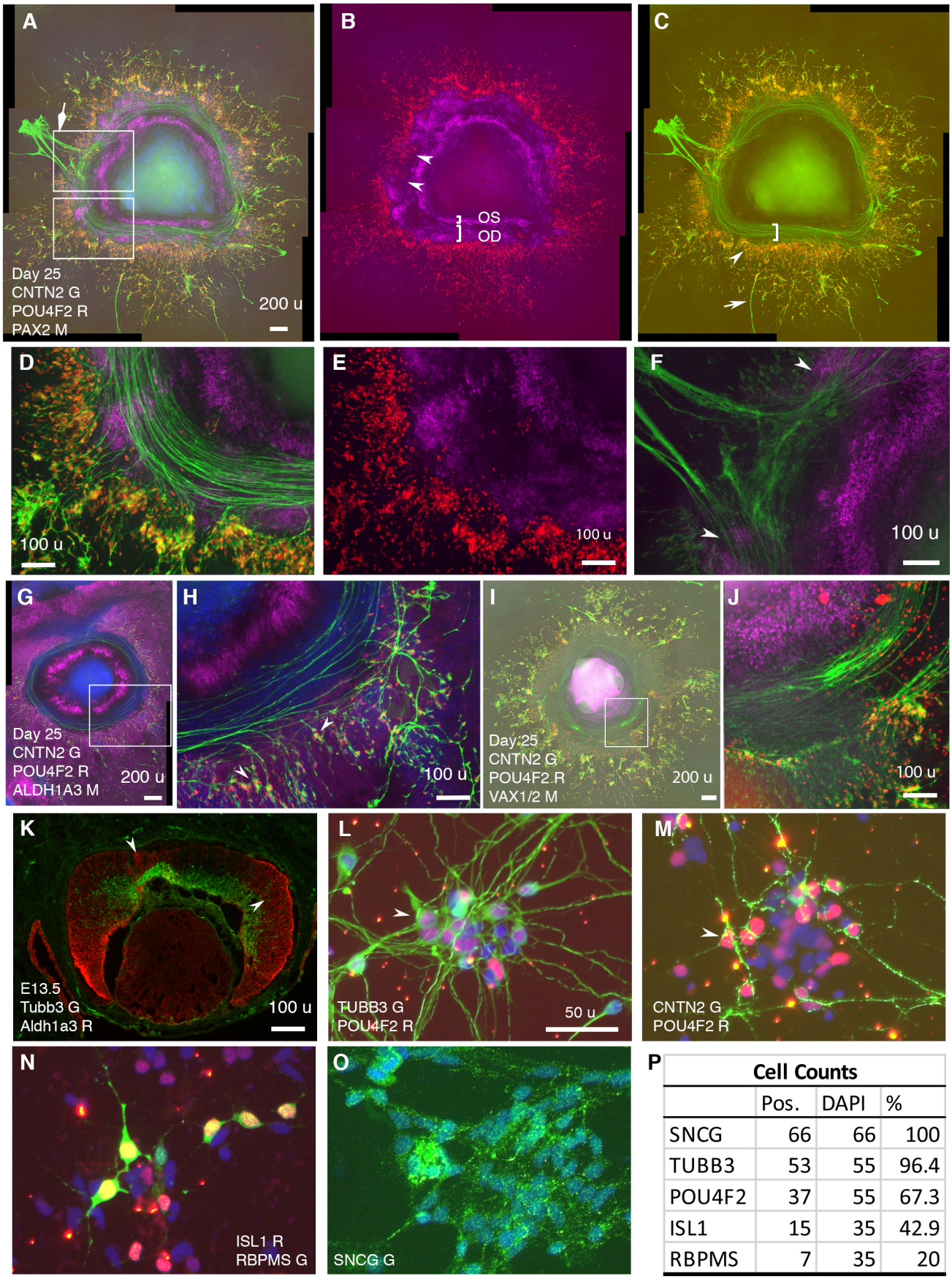

P

Cell Counts			
	Pos.	DAPI	%
SNCG	66	66	100
TUBB3	53	55	96.4
POU4F2	37	55	67.3
ISL1	15	35	42.9
RBPMS	7	35	20

Fig. 6

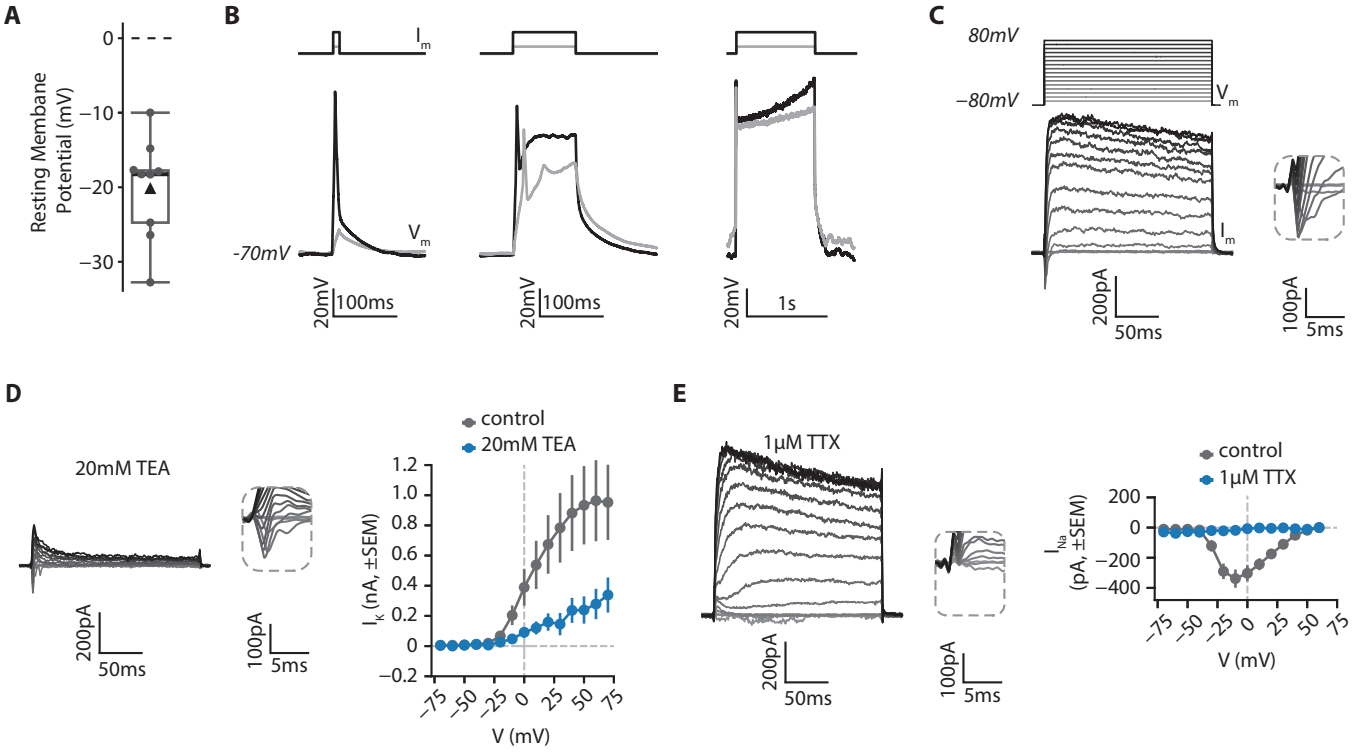
A
Resting Membane Potential (mV)
0
−10
−20
−30
B
I_m
V_m
-70mV
20mV
100ms
20mV
100ms
20mV
1s
C
80mV
−80mV
V_m
I_m
200pA
50ms
100pA
5ms
D
20mM TEA
200pA
50ms
100pA
5ms
control
20mM TEA
I_K (nA, ±SEM)
1.2
1.0
0.8
0.6
0.4
0.2
0
−0.2
−75
−50
−25
0
25
50
75
V (mV)
E
1μM TTX
200pA
50ms
100pA
5ms
control
1μM TTX
I_{Na} (pA, ±SEM)
200
0
−200
−400
−75
−50
−25
0
25
50
75
V (mV)

Fig. 7

A

gene	p_val	avg_logFC	pct.1	pct.2	p_val_adj	cluster
PAX2	0	0.930533006	0.769	0.169	0	2
FGF9	0	0.784668891	0.69	0.161	0	2
FGF8	1.77E-213	0.465810314	0.381	0.07	5.94E-209	2

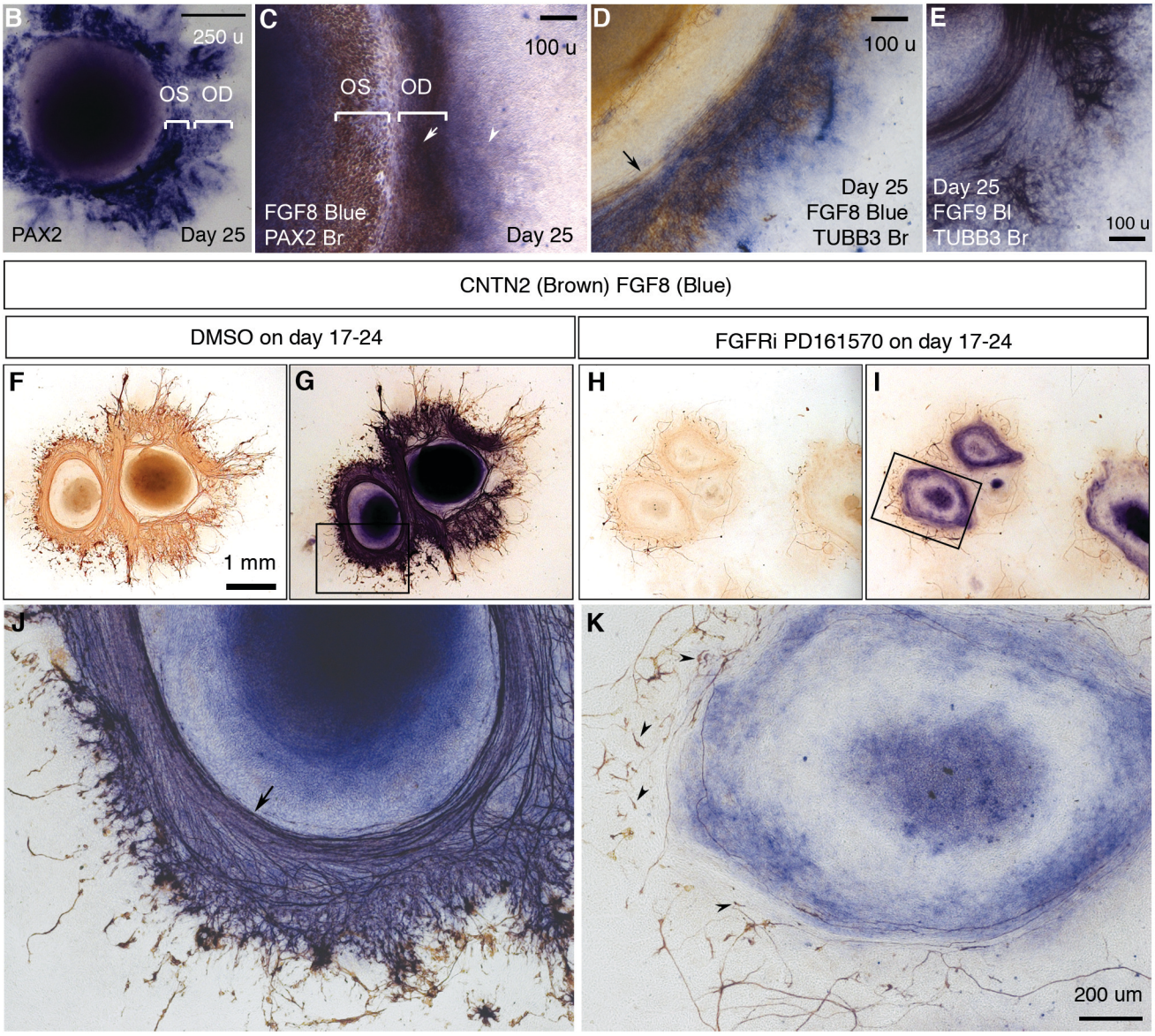

Tab.1. Cell counts of clusters in the scRNA-seq dataset

Cluster	0	1	2	3	4	5	6	7	8	9	10	11	12	13
Idents	Tel/R	Tel	OD	Tel	Tel/OS	NR	RPE	NR	Tel/OS	Tel/OS	Tel	RGC	Tel	UD
# Cells	1295	1158	964	931	921	871	747	743	729	603	450	393	333	80

Abbreviations: Idents, assigned cell identities; # Cells, cell number; Tel, telencephalon; R, retina; OD, optic disc; OS, optic stalk; RPE, retina pigment epithelium; RRG, retinal ganglion cell; UD, undetermined.